Environmental Science & Technology

pubs.acs.org/est

Article

Monthly Global Estimates of Fine Particulate Matter and Their Uncertainty

Aaron van Donkelaar,* Melanie S. Hammer, Liam Bindle, Michael Brauer, Jeffery R. Brook, Michael J. Garay, N. Christina Hsu, Olga V. Kalashnikova, Ralph A. Kahn, Colin Lee, Robert C. Levy, Alexei Lyapustin, Andrew M. Sayer, and Randall V. Martin

Cite This: *Environ. Sci. Technol.* 2021, 55, 15287−15300

Read Online

ACCESS | Metrics & More | Article Recommendations | Supporting Information

ABSTRACT: Annual global satellite-based estimates of fine particulate matter ($PM_{2.5}$) are widely relied upon for air-quality assessment. Here, we develop and apply a methodology for monthly estimates and uncertainties during the period 1998−2019, which combines satellite retrievals of aerosol optical depth, chemical transport modeling, and ground-based measurements to allow for the characterization of seasonal and episodic exposure, as well as aid air-quality management. Many densely populated regions have their highest $PM_{2.5}$ concentrations in winter, exceeding summertime concentrations by factors of 1.5−3.0 over Eastern Europe, Western Europe, South Asia, and East Asia. In South Asia, in January, regional population-weighted monthly mean $PM_{2.5}$ concentrations exceed 90 $\mu g/m^3$, with local concentrations of approximately 200 $\mu g/m^3$ for parts of the Indo-Gangetic Plain. In East Asia, monthly mean $PM_{2.5}$ concentrations have decreased over the period 2010−2019 by 1.6−2.6 $\mu g/m^3$/year, with decreases beginning 2−3 years earlier in summer than in winter. We find evidence that global-monitored locations tend to be in cleaner regions than global mean $PM_{2.5}$ exposure, with large measurement gaps in the Global South. Uncertainty estimates exhibit regional consistency with observed differences between ground-based and satellite-derived $PM_{2.5}$. The evaluation of uncertainty for agglomerated values indicates that hybrid $PM_{2.5}$ estimates provide precise regional-scale representation, with residual uncertainty inversely proportional to the sample size.

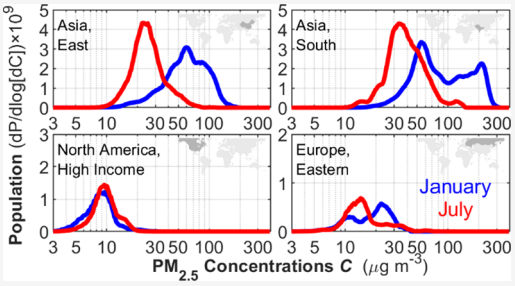

KEYWORDS: *fine particulate matter, aerosol optical depth, chemical transport model, satellite, air pollution*

■ INTRODUCTION

Outdoor fine particulate matter ($PM_{2.5}$) is the leading global environmental determinant of health, with millions of attributable deaths each year.[1] Despite the importance of $PM_{2.5}$, only 10% of countries have more than three ground-based $PM_{2.5}$ monitors per million people.[2] A geophysical-hybrid combination of satellite retrievals, chemical transport modeling, and ground monitor-based calibration can, however, provide quality long-term global[3,4] and regional[5] estimates of $PM_{2.5}$ concentrations. While high-quality $PM_{2.5}$ estimates using alternative methods can be produced using similar information sources in regions with dense monitoring networks,[6−8] this geophysical-hybrid (hereafter "hybrid") approach has been demonstrated to be effective even with sparse ground-based observation,[9] making it well suited for global air-quality applications.

These hybrid $PM_{2.5}$ datasets have proven to be a valuable source of information for epidemiological and health-impact assessments of $PM_{2.5}$ exposure.[1,10−13] Such studies have often focused on chronic (i.e., 1 year or longer) exposure, although impacts of $PM_{2.5}$ exposure at shorter timescales are important to consider and have been observed in in-utero infant development.[14,15] Resolving the differences in exposure impact among early lifetime windows, pre- and postnatal, is an increasingly important issue in identifying critical windows of risk that can have lifelong consequences.[16] These subannual exposures have the potential of presenting a unique global health burden in regions with seasonal variations in $PM_{2.5}$,[17−19] for which the current hybrid annual average exposures are less applicable, thus motivating a need for global $PM_{2.5}$ estimates with a subannual temporal resolution.

Understanding the uncertainty of $PM_{2.5}$ estimates when characterizing its associations with health impacts is important to ensure findings' significance. Uncertainty in purely geophysical $PM_{2.5}$ is affected by the accuracy of the satellite-retrieved total column aerosol optical depth (AOD) as well as the simulated AOD to the $PM_{2.5}$ relationship,[20,21] η. The hybrid approach additionally incorporates $PM_{2.5}$ observations

Received: August 9, 2021
Revised: September 27, 2021
Accepted: September 29, 2021
Published: November 1, 2021

https://doi.org/10.1021/acs.est.1c05309
Environ. Sci. Technol. 2021, 55, 15287−15300

from ground-based monitors to reduce this uncertainty by adjusting geophysical values based on statistical associations with relevant factors, such as the aerosol type or local terrain. To be meaningful in this context, uncertainty-related factors must represent limitations of properties or processes important for the calculation of the AOD or η. The role of uncertainty in $PM_{2.5}$ exposure when characterizing global health impacts has not been well explored, in part due to insufficient $PM_{2.5}$ uncertainty estimates. A direct estimate of uncertainty would allow for better characterization of exposure to directly examine study limitations.

Here, we improve and extend our previous annually based work[3,22] to provide global hybrid $PM_{2.5}$ estimates from 1998 to 2019 at a monthly timescale. These improvements include a resolution-tiered approach for retaining fine resolution while combining multiple AOD datasets, representation of missing or limited ground-based monitor data for monthly evaluation, additional observation-based predictor variables of residual bias in $PM_{2.5}$ estimates, and temporal variation in predictor coefficients at a global scale. Additionally, we develop an estimate of per-pixel uncertainty based on relevant geophysical factors. We then go on to evaluate these results and summarize regional $PM_{2.5}$ concentrations and trends by season.

■ DATA SOURCES AND METHODS

Our hybrid $PM_{2.5}$ estimates are primarily determined by geophysical estimates of $PM_{2.5}$ from the AOD using a physically based relationship between the AOD and $PM_{2.5}$ that is represented by η. Geophysical accuracy relies on the quality of both AOD and η. Hybrid $PM_{2.5}$ improves upon geophysical $PM_{2.5}$ by the statistical interpretation of differences between geophysical and observed $PM_{2.5}$ at monitored locations using predictor variables that are associated with geophysical estimates and can be applied for global adjustments.

Resolution-Tiered Approach to Produce the "Best-Estimate" AOD. Daily AOD retrievals from each satellite-based data set were transformed onto a regular 0.1° × 0.1° grid and averaged to data set-specific monthly means. To reduce sampling effects, daily values absent from individual retrievals are approximated using the average of available retrievals on missing days, scaled by their monthly climatological ratio to the missing values. The simulated ratio of all days within a month to the sampled days is lastly applied to account for days during which no retrieval was available. Following our previous approach,[3,22] these monthly AOD retrieval means (AOD_k) were combined to produce a monthly best-estimate satellite-based AOD at 0.1° × 0.1° ($AOD_{BE,SAT}$) using a weighted average based on the level of agreement with AERONET. Specifically, the weight of each term is defined as follows:

$$W_k = NRMSD_k^{-1} \times \frac{AOD_k}{(AOD_{adj,k} - AOD_k)} \quad (1)$$

where $NRMSD_k$ and $AOD_{adj,k}$ are the normalized root-mean-square difference and regression-slope-adjusted AOD, respectively. $NRMSD_k$ is capped at a value of 1. Details of the AOD retrievals used and their comparison with AERONET are provided in Supporting Information Section S1.

$AOD_{BE,SAT}$ was then averaged to local simulation resolution (0.5° × 0.625° over North America, Europe, and Asia or 2° × 2.5° globally) and combined with simulated AOD following eq 1 to produce an overall best estimate AOD at a simulation resolution ($AOD_{BE,SIMRES}$). The weight (W_k) of $AOD_{BE,SAT}$ at the simulation resolution within eq 1 was represented as the average per-pixel sum of the individual AOD retrieval weights for $AOD_{BE,SAT}$ within each simulation-grid cell. The best estimate all-source AOD at 0.1° × 0.1° ($AOD_{BE,0.1°}$) was then determined by applying the difference between $AOD_{BE,SAT}$ and its average at simulation resolution. Differences between the climatological monthly mean MAIAC AOD at 0.01° × 0.01° and 0.1° × 0.1° were then similarly applied to $AOD_{BE,0.1°}$ to produce the best estimate AOD at 0.01° × 0.01° (AOD_{BE}). This resolution-tiered approach provides the advantages of using multiple AOD datasets at their appropriate resolution, while also including fine-scale features not universally captured. Satellite observations comprise most (90.7−96.3%) of the population-weighted AOD_{BE} and vary with seasonal conditions such as cloud and snow cover (Supporting Information, Figure S1).

Geophysical $PM_{2.5}$ Estimates. We relate AOD_{BE} to monthly mean $PM_{2.5}$ using the geophysical relationship simulated using the GEOS-Chem chemical transport model[23] (http://geos-chem.org; V11−01; using simulation-specific details and updates described by Hammer et al.[3]):

$$PM_{2.5} = \eta\,(x, y, t) \times AOD_{BE} \quad (2)$$

where η is the spatially and temporally varying ratio between the monthly mean AOD at AOD sampling time and 24 h monthly mean $PM_{2.5}$. The representative sampling time of AOD_{BE} is determined by the relative weights of individual AOD datasets based on their respective sampling times and the geophysical relationship used to account for diel effects. This factor includes the impact of aerosol vertical structures and optical properties on the relationship between AOD and $PM_{2.5}$ via the GEOS-Chem simulated representation of physics, chemistry, and transport within the atmosphere. Effects of sampling time, emissions, composition, hygroscopicity, and local meteorological factors such as the relative humidity, boundary layer height, wind speed, and wind direction are included in the GEOS-Chem calculation of the AOD to $PM_{2.5}$ relationship.

Incorporation of Ground-Based Observations. Ground-based observations are used to improve geophysical $PM_{2.5}$ estimates by interpreting the observed differences between geophysical and monitor-based $PM_{2.5}$. Over North America, we obtained $PM_{2.5}$ observations from the United States' Environmental Protection Agency's Air Quality System (AQS) and Environment Canada's National Air Pollution Surveillance (NAPS) program. Federal Reference Method and non-Federal Reference Methods $PM_{2.5}$ were included. Fine mass from the IMPROVE network is adjusted for the observed changes in particle-bound water.[24] Over Europe, we use $PM_{2.5}$ measurements available from the European Environment Agency Air Quality e-Reporting system (https://www.eea.europa.eu/data-and-maps/data/aqereporting). Over mainland China, $PM_{2.5}$ measurements were obtained from http://beijingair.sinaapp.com/. These data are captured by individuals from instantaneous data records on the website of the Chinese Environmental Protection Agency. $PM_{2.5}$ measurements from the Taiwanese Environmental Protection Agency were downloaded from https://taqm.epa.gov.tw/taqm/tw/YearlyDataDownload.aspx. Australian observations were separately downloaded for the Northern Territory (http://ntepa.webhop.net/NTEPA/), Queensland (https://www.data.qld.gov.au/dataset/), and New South Wales (https://www.dpie.

https://doi.org/10.1021/acs.est.1c05309
Environ. Sci. Technol. 2021, 55, 15287−15300

nsw.gov.au/air-quality/air-quality-data-services/data-download-facility). We additionally use values from literature-based observations, the World Health Organization Global Ambient Air Quality Database,[25] and as available from OpenAQ (http://openaq.org), which provide coverage from locations around the world, including the Surface Particulate Matter Network (SPARTAN[26,27]).

The spatial and temporal availability of ground-based monitors varies by regions, and duplication across some databases is possible, with the potential to impact their incorporation with geophysical $PM_{2.5}$. We address duplications by combining collocated data. Reported monthly measurements at a site also offer information about neighboring sites. In order to leverage available monthly measurements, we combine the available monthly means of ground-based observations to propagate monthly information to monitor locations with missing values. While these inferred observations have increased uncertainty, they offer increased long-term spatiotemporal stability where direct observation is absent.

Briefly, the agreement between each monitor site and other monitor locations, as well as geophysical and GEOS-Chem simulated $PM_{2.5}$ are determined and used to infer missing values at monitor locations where a direct observation is unavailable for a given month. Details of this algorithm are given in Supporting Information Section S2. The resultant inferred values show good cross-validated agreement when all data sources are used (R^2 = 0.99; Supporting Information Figure S2a), where cross-validation is obtained by withholding the individual value at a month and location and the inferred result compared with the original observation. The inferred values based solely on geophysical and simulated $PM_{2.5}$, representative of earlier years with fewer direct observations, also show good cross-validated agreement (R^2 = 0.92; Supporting Information Figure S2b). Example timeseries of selected locations at monitored locations are given in Supporting Information Figure S3.

Monthly Hybrid $PM_{2.5}$ Estimates. We incorporate these ground-based $PM_{2.5}$ values at a monthly timescale using a geographically weighted regression (GWR[28]) with predictor variables primarily related to the uncertainties in η. Following our previous work,[3,22] we define compositionally based predictors by applying the simulated relative contribution of sulfate, nitrate, organic carbon, secondary organics, sea salt, and mineral dust to the geophysical $PM_{2.5}$ estimate. These predictors are associated with errors in η potentially caused by simulation uncertainties of emissions, chemistry, optics, and transport.

We define additional predictors associated with increased potential for uncertainty in η, as represented by the difference between the simulated and retrieved AOD at simulation scales ($PM_{2.5}{}'_{BIAS}$), as well as large vertical gradients in η ($PM_{2.5}{}'_{PROFILE}$). Additional predictors, associated with features that occur below simulation-grid resolution that may result in local η biases include topographic features at a subgrid scale ($PM_{2.5}{}'_{SGTOPO}$), aerosol features at a subgrid scale ($PM_{2.5}{}'_{SGA}$), and coastal effects at a subgrid scale ($PM_{2.5}{}'_{COASTAL}$). The details of these parameters are given in Supporting Information Section S3.

Uncertainty of Monthly Hybrid $PM_{2.5}$ Estimates. We represent the uncertainty in hybrid $PM_{2.5}$ ($PM_{2.5}{}'_{hyb}$) using the range of $PM_{2.5}$ values obtained by the variation among, or the uncertainty common to, the individual AOD datasets that were used to determine AOD_{BE}. We additionally include the sensitivity of the GWR-based adjustment to monitor selection and weight as a means to account for uncertainty related to the AOD, η, and observed values themselves.

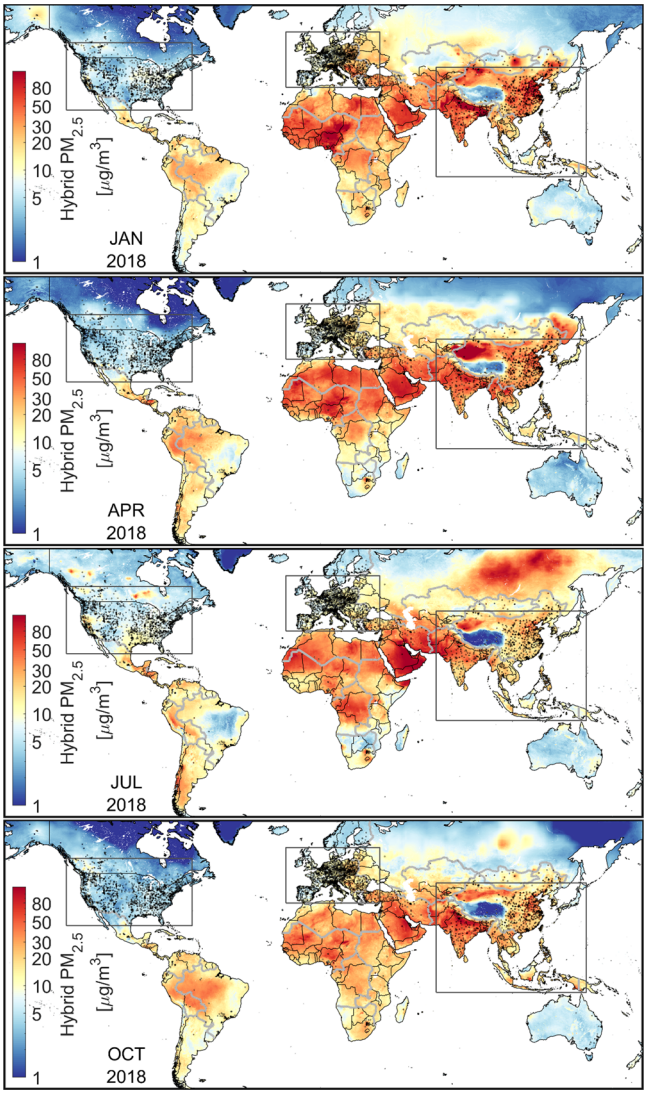

Figure 1. Global monthly mean $PM_{2.5}$ for January, April, July, and October 2018. Circles correspond to ground monitor locations. Thin black lines represent country boundaries and shorelines. Thick gray lines represent regions used by the GBD[1] study. Black boxes represent regions used in Figure 2 and Table 1.

Specifically, we represent the direct impact of per-pixel AOD uncertainty on hybrid $PM_{2.5}$ estimates by applying the geophysical relationship between the AOD and $PM_{2.5}$ (η) to the uncertainty in the AOD:

$$PM_{2.5}{}'_{AOD} = \eta\,(x, y, t) \times AOD_{BE}{}' \tag{3}$$

where $PM_{2.5}{}'_{AOD}$ is the uncertainty in hybrid $PM_{2.5}$ associated with the direct AOD uncertainty. $AOD_{BE}{}'$ is the uncertainty of each AOD_{BE} pixel, which we represent as the largest of the following:

1) The absolute difference between a bias-adjusted and bias-unadjusted AOD_{BE}, $|AOD_{BE,adj} - AOD_{BE}|$. The adjusted AOD ($AOD_{BE,adj}$) was produced by applying the local regression slopes determined from AERONET to each satellite-based and simulation-based AOD data

https://doi.org/10.1021/acs.est.1c05309
Environ. Sci. Technol. 2021, 55, 15287−15300

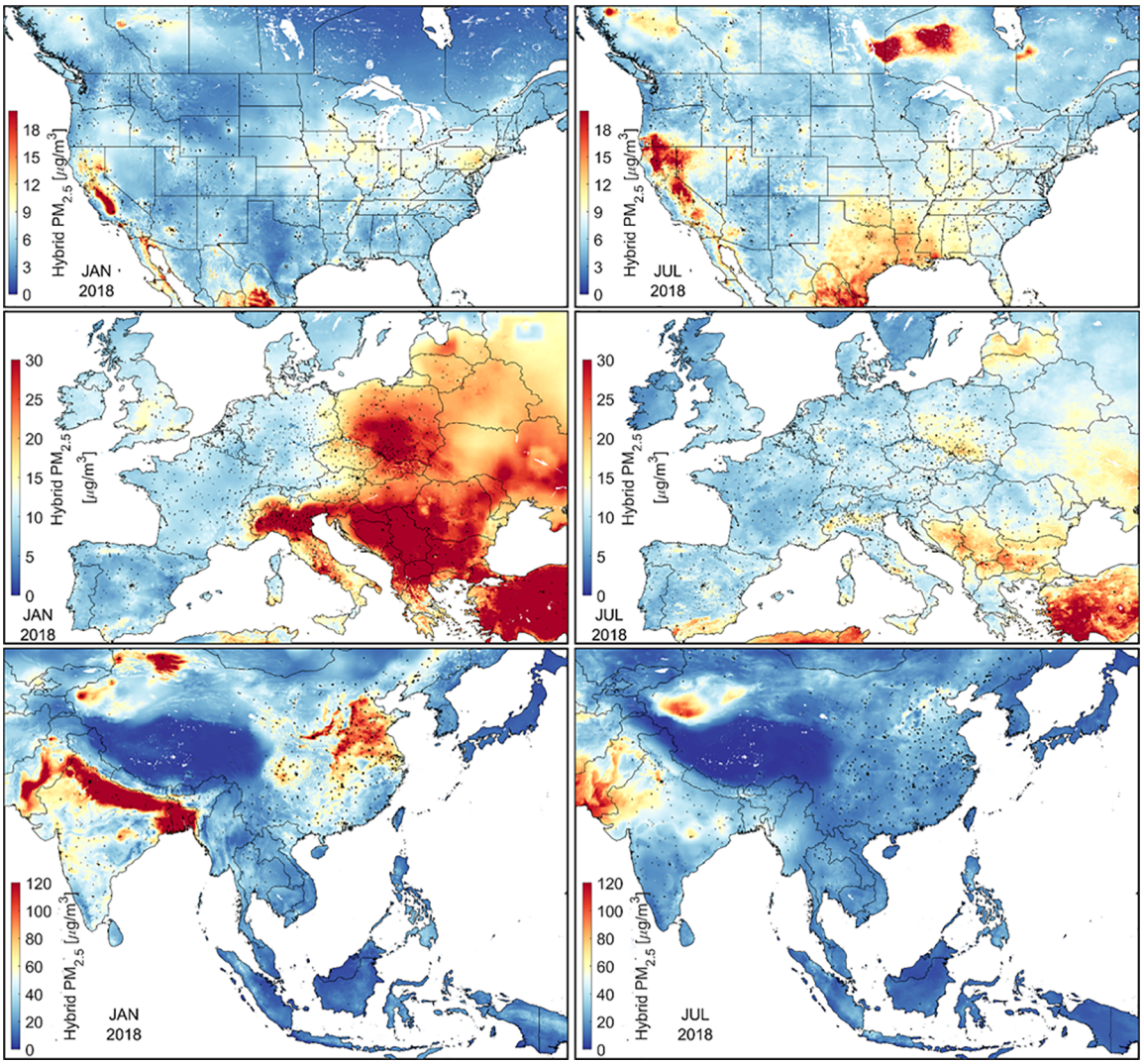

Figure 2. Regional monthly mean $PM_{2.5}$ for January (left column) and July (right column) 2018. Circles correspond to ground monitor locations. Thin black lines represent country boundaries and shorelines. Thick gray lines represent the GBD regional boundaries.

set prior to their combination, following the above-mentioned method.

2) The one-sigma AOD range, based on the weighted percentile of the individual AOD_{BE} source datasets, where percentile weights are defined according to eq 1.
3) The residual variance between the $AOD_{BE,adj}$ and AERONET AOD.
4) A percentage (0.02 + 15%) of the combined AOD value, where 0.02 is taken from one-sigma error of AERONET observations[29] and 15% from the relative contribution to the error envelopes observed for several input AOD retrievals.[30−32]

The per-pixel sensitivity of the GWR-based adjustment is calculated using the combined impact of variability in the compositional and noncompositional GWR predictor coefficients when added in quadrature:

$$PM_{2.5}{}'_{GWR} = \left(\sum \sigma_x{}^2\right)^{1/2} \tag{4}$$

where σ_x is the standard deviation of the adjustment from each GWR predictor variable during 10-fold cross-validation and randomly varying monitor weights by up to 50%.

By design, $PM_{2.5}{}'_{GWR}$ includes an estimate of uncertainty from both the AOD and η, but is more sensitive to $PM_{2.5}$ ground monitor placement than $PM_{2.5}{}'_{AOD}$. We therefore treat the overall hybrid $PM_{2.5}$ uncertainty, $PM_{2.5}{}'_{hyb}$, as the maximum of $PM_{2.5}{}'_{AOD}$, $PM_{2.5}{}'_{GWR}$, and 1 $\mu g/m^3$ + 15% of hybrid $PM_{2.5}$:

$$PM_{2.5}{}'_{hyb} = \max(PM_{2.5}{}'_{AOD}, PM_{2.5}{}'_{GWR}, 1\ \mu g/m^3 + 15\% \times \text{hybrid } PM_{2.5}) \tag{5}$$

where 1 $\mu g/m^3$ + 15% × hybrid $PM_{2.5}$ follows the AOD-related uncertainty represented by (eq 4) above and ensures that uncertainty does not approach zero under low-η conditions.

Population estimates, which are applied for the interpretation of results, are based on the Gridded Population of the World (GPW v4) database[33] for 2015.

RESULTS AND DISCUSSION

Figure 1 shows the global monthly mean hybrid $PM_{2.5}$ in January, April, July, and October 2018. Regional maps for January and July over North America, Europe, and Asia are shown in Figure 2. The two left columns of Table 1 summarize

https://doi.org/10.1021/acs.est.1c05309
Environ. Sci. Technol. 2021, 55, 15287−15300

Table 1. Comparison of Annual and Monthly Mean Cross-Validated Hybrid and Monitor-Based $PM_{2.5}$[a]

region/ month	geographic mean $PM_{2.5}$ [$\mu g/m^3$]	population-weighted mean $PM_{2.5}$ [$\mu g/m^3$]	population-weighted co-monitor[b] mean $PM_{2.5}$ [$\mu g/m^3$]	population-weighted monitor mean $PM_{2.5}$ [$\mu g/m^3$]	R^2	R^2 with WHO-collocated monitors	RMSE [$\mu g/m^3$]	slope	number of monitor locations	number of WHO monitor locations	comparison year range
global											
annual	19.3 [18.9, 20.1]	35.9 [34.6, 37.7]	22.7 [21.2, 24.6]	23.1 [21.6, 25.0]	0.84 [0.81, 0.86]	0.94 [0.93, 0.95]	8.4 [8.3, 8.5]	1.00 [0.98, 1.01]	11,015	4409	2015−2019
JAN	20.8 [20.1, 22.2]	50.3 [49.1, 52.5]	32.0 [29.2, 35.2]	32.7 [30.1, 36.0]	0.86 [0.84, 0.88]	0.93 [0.92, 0.95]	13.3 [13.2, 13.4]	1.01 [0.99, 1.02]	11,015	4409	2015−2019
APR	19.7 [18.7, 20.9]	34.1 [32.9, 36.2]	21.1 [20.2, 22.5]	21.4 [20.5, 22.7]	0.81 [0.78, 0.84]	0.93 [0.90, 0.94]	8.5 [8.2, 8.6]	0.99 [0.97, 1.01]	11,015	4409	2015−2019
JUL	20.6 [19.2, 21.9]	26.7 [26.0, 28.2]	17.4 [16.4, 19.6]	17.6 [16.7, 19.8]	0.72 [0.67, 0.77]	0.88 [0.83, 0.91]	8.0 [7.6, 8.3]	0.98 [0.96, 0.99]	11,015	4409	2015−2019
OCT	17.4 [16.0, 18.9]	33.6 [32.0, 36.1]	20.9 [19.7, 24.4]	21.2 [19.9, 24.5]	0.78 [0.75, 0.82]	0.92 [0.89, 0.93]	9.7 [9.4, 9.9]	0.99 [0.97, 1.00]	11,015	4409	2015−2019
North America											
annual	6.5 [5.2, 7.6]	9.8 [7.7,1 2.0]	8.7 [6.9, 10.5]	8.8 [6.9, 10.6]	0.57 [0.42, 0.73]	0.67 [0.52, 0.82]	2.1 [1.8, 2.2]	0.99 [0.98, 1.00]	2795	1358	2001−2019
JAN	6.3 [5.2, 8.4]	10.3 [7.9, 14.8]	9.2 [7.3, 13.0]	9.4 [7.4, 13.2]	0.51 [0.29, 0.64]	0.60 [0.32, 0.76]	3.1 [2.7, 3.9]	0.99 [0.98, 1.00]	2795	1358	2001−2019
APR	5.9 [4.4, 7.2]	8.8 [6.7, 11.2]	7.6 [5.7, 9.5]	7.6 [5.7, 9.5]	0.57 [0.44, 0.71]	0.63 [0.47, 0.78]	2.0 [1.8, 2.3]	0.97 [0.96, 0.98]	2795	1358	2001−2019
JUL	8.4 [5.8, 11.2]	11.4 [8.4, 15.0]	10.1 [7.3, 13.1]	10.0 [7.3, 13.1]	0.61 [0.43, 0.78]	0.68 [0.44, 0.86]	2.7 [2.1, 4.3]	0.98 [0.96, 1.00]	2795	1358	2001−2019
OCT	5.7 [4.4, 7.0]	8.5 [6.5, 11.2]	7.7 [6.0, 9.7]	7.7 [6.0, 9.7]	0.53 [0.42, 0.69]	0.61 [0.49, 0.80]	2.2 [1.9, 2.6]	0.98 [0.96, 0.99]	2795	1358	2001−2019
Europe											
annual	15.5 [14.3, 17.1]	16.3 [15.0, 18.3]	15.8 [14.2, 18.3]	16.0 [14.4, 18.5]	0.68 [0.66, 0.70]	0.73 [0.71, 0.74]	4.3 [4.1, 4.6]	0.99 [0.99, 1.00]	3184	1060	2010−2019
JAN	21.1 [18.4, 25.4]	21.7 [18.7, 27.0]	22.0 [18.2, 29.4]	22.3 [18.5, 29.8]	0.72 [0.67, 0.76]	0.73 [0.65, 0.79]	7.2 [6.4, 8.4]	1.00 [0.99, 1.02]	3184	1060	2010−2019
APR	14.9 [12.7, 16.8]	15.7 [13.7, 18.3]	14.7 [12.4, 17.7]	14.8 [12.4, 17.7]	0.59 [0.53, 0.64]	0.62 [0.53, 0.70]	4.4 [4.1, 4.7]	0.98 [0.97, 0.99]	3184	1060	2010−2019
JUL	12.1 [10.9, 14.0]	12.7 [11.5, 14.1]	12.0 [10.5, 13.8]	12.0 [10.6, 13.9]	0.53 [0.42, 0.58]	0.50 [0.37, 0.59]	3.6 [3.4, 3.8]	0.98 [0.97, 0.98]	3184	1060	2010−2019
OCT	14.4 [12.0, 16.0]	15.4 [13.5, 17.1]	15.3 [13.3, 17.5]	15.5 [13.7, 17.8]	0.67 [0.62, 0.71]	0.74 [0.66, 0.79]	4.8 [4.4, 5.1]	0.99 [0.98, 1.00]	3184	1060	2010−2019
Asia											
annual	31.3 [29.9, 33.6]	45.9 [44.2, 47.9]	43.4 [39.7, 48.0]	43.9 [40.2, 48.5]	0.69 [0.65, 0.72]	0.87 [0.86, 0.88]	11.9 [11.7, 12.2]	1.00 [0.99, 1.01]	3437	1641	2015−2019
JAN	38.7 *[36.4, 41.1]*	68.7 [66.8, 70.4]	66.5 [60.6, 73.5]	67.9 [62.3, 74.6]	0.75 [0.72, 0.80]	0.86 [0.84, 0.90]	20.5 [19.5, 20.9]	1.01 [1.00, 1.03]	3437	1641	2015−2019
APR	34.4 [32.1, 38.1]	42.4 [40.6, 44.0]	40.6 [36.8, 44.3]	41.1 [37.3, 44.8]	0.62 [0.58, 0.66]	0.81 *[0.78, 0.84]*	11.7 [11.1, 12.0]	1.00 [0.98, 1.01]	3437	1641	2015−2019
JUL	24.3 [22.6, 27.7]	30.4 [28.8, 33.1]	28.8 [25.6, 34.0]	28.9 [25.8, 34.1]	0.59 [0.49, 0.65]	0.81 [0.70, 0.86]	9.4 [8.9, 10.0]	0.98 [0.95, 0.99]	3437	1641	2015−2019
OCT	29.2 [27.2, 34.1]	43.8 [42.3, 47.5]	39.5 [36.3, 47.2]	39.8 [36.7, 47.3]	0.61 [0.57, 0.64]	0.83 [0.75, 0.87]	14.6 [14.1, 14.8]	0.99 [0.97, 1.00]	3437	1641	2015−2019

[a]Mean [min, max] values are given. [b]Pixels containing a ground-based monitor.

https://doi.org/10.1021/acs.est.1c05309
Environ. Sci. Technol. 2021, 55, 15287−15300

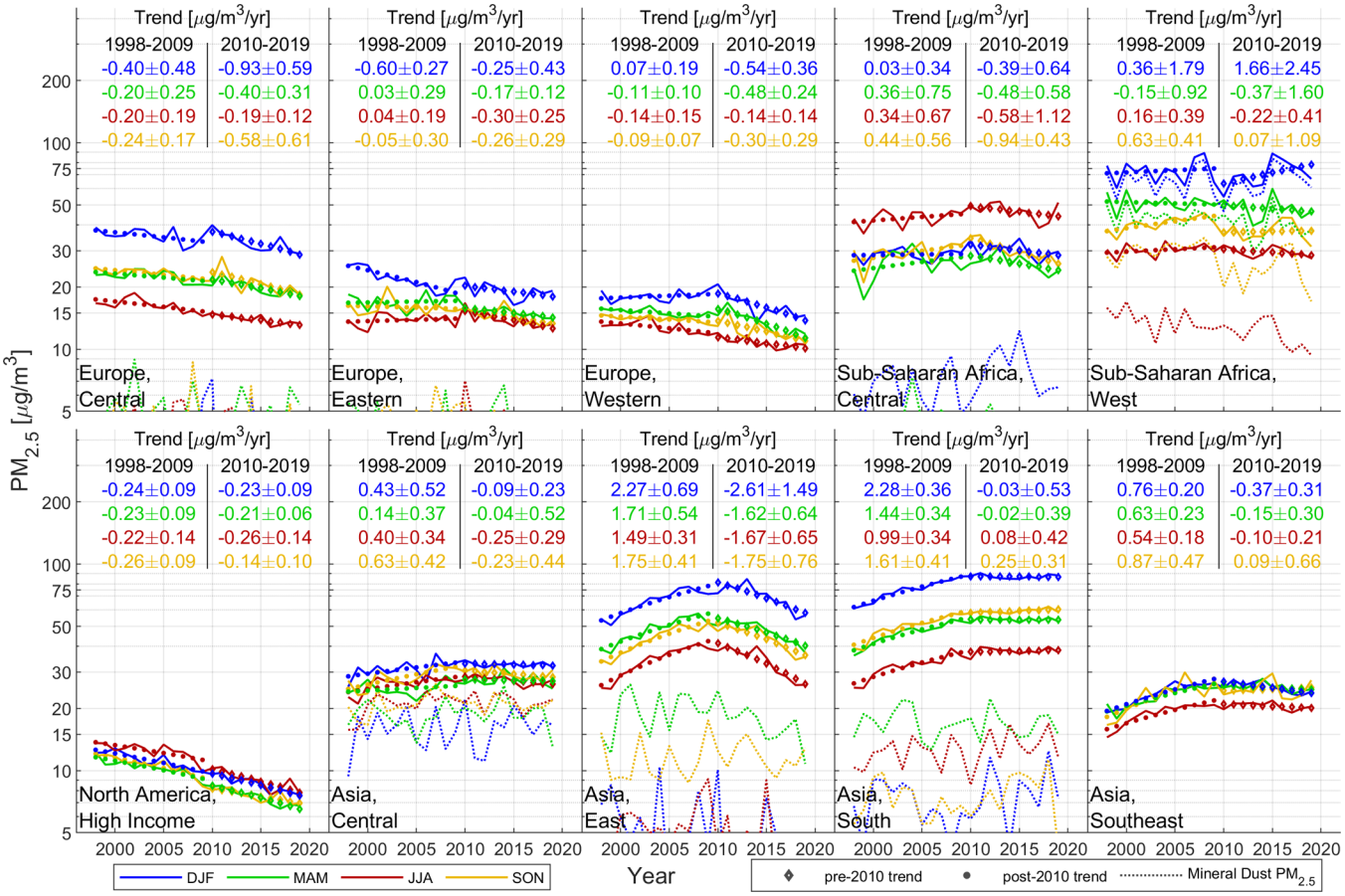

Figure 3. Mean population-weighted $PM_{2.5}$ concentrations and trends for DJF (blue), MAM (green), JJA (red), and SON (yellow) over the selected GBD regions. Dots and diamonds correspond to the 1998−2009 and 2010−2019 trends within each panel, with color-matched values and 95% confidence intervals given in $\mu g/m^3$/year. Dashed lines show the estimated contribution of mineral dust to the population-weighted $PM_{2.5}$ concentrations. Supporting Information Table S3 summarizes monitor-collocated trends.

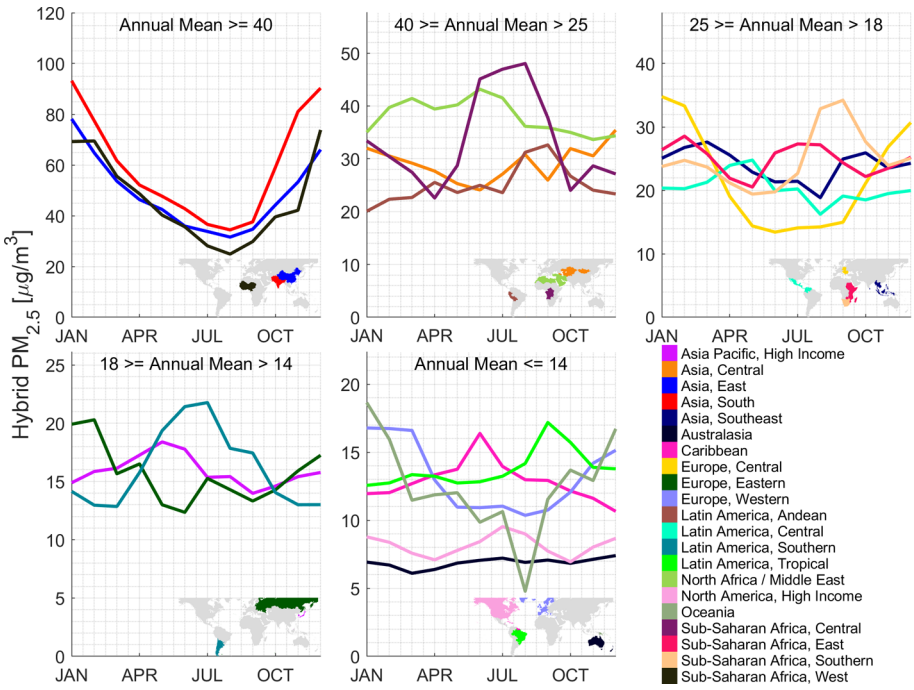

Figure 4. Average population-weighted monthly mean $PM_{2.5}$ variation by region, 2010−2019. Regions are sorted by average annual mean $PM_{2.5}$, as indicated within each panel.

https://doi.org/10.1021/acs.est.1c05309
Environ. Sci. Technol. 2021, 55, 15287−15300

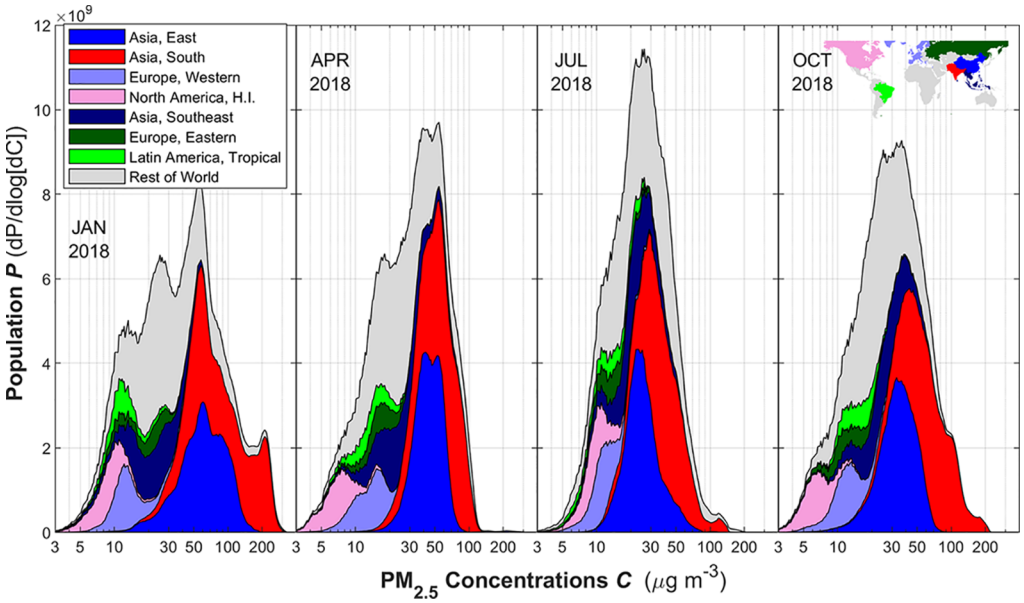

Figure 5. Regional distributions of population as a function of $PM_{2.5}$ concentration for January, April, July, and October 2018. Plotted data show bin-width normalized distributions over 400 logarithmically spaced bins such that equal-size areas represent equal populations.

the mean $PM_{2.5}$ over these regions. Large variabilities in seasonal concentrations are visible, such as biomass burning-driven features in summer (July) over northern and western North America and northern Asia. Over parts of China and South Asia, wintertime (January) population-weighted concentrations were more than double summertime concentrations. The Indo-Gangetic Plain, for example, has January monthly mean $PM_{2.5}$ concentrations of around 180 $\mu g/m^3$ compared to 50 $\mu g/m^3$ or less in July. $PM_{2.5}$ concentrations generally differ by more than a factor of two between eastern and western Europe during winter months compared to a factor of about 20% in summer. The analysis of ground-based observations corroborates the pronounced seasonal $PM_{2.5}$ variation over China,[34,35] India,[36−38] and Eastern Europe[39,40] with attribution to wintertime burning of solid fuels,[39] shallow mixed layers,[41] favorable thermodynamics for nitrate,[42] and rapid sulfate production.[43]

Extended regional monthly maps are provided in Supporting Information Figure 4a−k, showing features beyond those highlighted above. Biomass burning produces significant seasonal enhancements in $PM_{2.5}$ around the world and is related to increased concentrations during the dry season in Central America (February−May), peat fires during September−October in Indonesia,[44] and land-use practices in Central Africa.[45] High $PM_{2.5}$ concentrations in the Amazon from August to October are consistent with dry season burning,[46] with lower concentrations during the wet season.[47] Desert dust emissions and transport also have a major influence on $PM_{2.5}$ seasonal cycles and are related to increased $PM_{2.5}$ concentrations over the Middle East in July,[48] the Sahara in April,[49] and Nigeria in January.[50] Seasonal variations in Australia are complex and driven by smoke, mineral dust, and marine aerosol.[51]

Table 1 additionally compares monthly mean hybrid $PM_{2.5}$ concentrations with collocated ground-based observations for time periods during which each region had well-established ground-based observational networks. Supporting Information Figure S5 shows these comparisons for January and July 2018. Hybrid $PM_{2.5}$ estimates exhibit general consistency with ground-based observations over all seasons and regions, with the relative performance of R^2 versus Root Mean Square Error (RMSE) reflecting the regional $PM_{2.5}$ distribution, such as the regions of lower $PM_{2.5}$ concentrations, demonstrating higher fractional differences. Regionally, the monthly R^2 values between the hybrid and monitor-based $PM_{2.5}$ over Europe (0.53−0.74) and Asia (0.59−0.86) are higher compared to those over North America (0.51−0.68), with the highest R^2 over Asia at the WHO-coincident locations (0.81−0.86), where measurements are most reliable. In contrast, RMSE is lowest over North America (2.0−3.1 $\mu g/m^3$), followed by Europe (3.6−7.2 $\mu g/m^3$) and Asia (9.4−20.5 $\mu g/m^3$). Globally, population-weighted mean $PM_{2.5}$ concentrations at ground-monitored locations closely agree with hybrid values (22.7 $\mu g/m^3$ vs 23.1 $\mu g/m^3$). Hybrid $PM_{2.5}$ concentrations, however, suggest a large difference between the population-weighted mean $PM_{2.5}$ at monitored locations and a complete global population-weighted mean value (22.7 $\mu g/m^3$ vs 35.9 $\mu g/m^3$), suggesting monitored locations underestimate $PM_{2.5}$ exposure at a global scale. The difference between population-weighted $PM_{2.5}$ at monitored and unmonitored locations is much smaller over North America, Europe, and Asia, suggesting that the need for additional ground-based observations is primarily outside these relatively well-monitored regions and greater throughout the Global South.

Supporting Information provides a comparison of these results with our previous annual global[3] (V4.GL.03; Table S1) and monthly regional[3,5] (V4.NA.03, V4.EU.03, and V4.CH.03; Table S2) datasets. Geographic and population-weighted regional mean $PM_{2.5}$ concentrations are similar across all datasets, but annual mean R^2 demonstrates significant regional improvements compared to V4.GL.03 over North America (R^2 = 0.58−0.75 versus R^2 = 0.41−0.53), Europe (R^2 = 0.69−0.81 versus R^2 = 0.48−0.60), and Asia (R^2 = 0.68−0.91 versus R^2 = 0.60−0.78). While these comparisons are limited by inconsistencies in cross-validation and monitor availability between versions, they suggest that this current work demonstrates an R^2 of at least as good, or better than previous regional $PM_{2.5}$ estimates over all regions. Improvements in

https://doi.org/10.1021/acs.est.1c05309
Environ. Sci. Technol. 2021, 55, 15287−15300

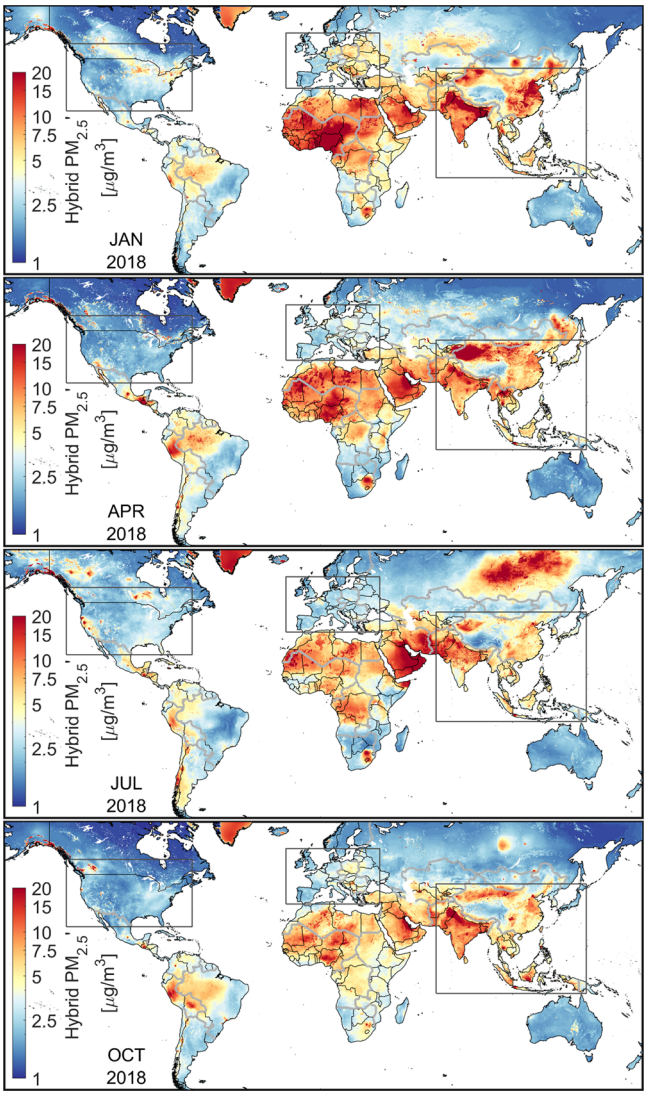

Figure 6. Per-pixel (1 km × 1 km) monthly mean hybrid $PM_{2.5}$ uncertainty for January, April, July, and October 2018. Thin black lines represent country boundaries and shorelines. Thick gray lines represent the Global Burden of Disease regions. Black boxes represent regions used in Figure 2 and Table 1. These values are shown as the percentage of $PM_{2.5}$ in Supporting Information, Figure S8.

performance reflect both the treatment of AOD, as evidenced by improved geophysical performance over North America and China, and calibration-related enhancements as evidenced by improved performance in hybrid $PM_{2.5}$ over Europe despite unchanged performance in geophysical $PM_{2.5}$ for Europe.

Of additional note is the impact of monitoring data quality on agreement, with the estimates agreeing with monitors included in the WHO database (shown in Supporting Information Figure S6) more than with the entire ground monitor data set. This impact likely represents increased uncertainties in both ground-based measurements and hybrid $PM_{2.5}$ concentrations at measurement sites not included in the WHO database and is apparent across all regions. This impact also highlights the importance of a consistent ground-truth database when evaluating multiple $PM_{2.5}$ datasets.

Figure 3 plots seasonal mean concentrations from 1998 to 2019 for several Global Burden of Disease[1] (GBD)-defined regions. The estimated contributions of mineral dust to $PM_{2.5}$ are also shown, calculated by applying the relative simulated compositional fraction to hybrid $PM_{2.5}$. Pre- and post-2010 trends separate previous and more recent $PM_{2.5}$ exposure trajectories. Substantial long-term variations were not observed over other GBD regions. Regional trends inferred from ground-based observations and hybrid $PM_{2.5}$ at monitor locations are generally consistent with regional trends, as demonstrated by Supporting Information, Table S3. As with previous analysis,[3] a major distinction between pre- and post-2010 trends occurs over East Asia. Notably, the monthly analysis presented here demonstrates that the East Asian peak in summertime $PM_{2.5}$ exposure occurs 2−3 years prior to the peak in wintertime exposure, which is consistent with an earlier timeline for decreases in SOx emissions[52] that contribute to summer sulfate enhancement over China, compared to NOx emissions[53] that contribute to winter nitrate enhancement. Although East Asian $PM_{2.5}$ remains among the highest in the world, 2019 summertime exposures decreased well below 30 $\mu g/m^3$ compared to 2007−2011 when summertime $PM_{2.5}$ was consistently near 40 $\mu g/m^3$. Wintertime exposures in this region remain high (>50 $\mu g/m^3$), but again show significant improvements in recent years. South Asian $PM_{2.5}$ exposure was similar to that of East Asian exposure at the turn of the millennium and exhibited similar upward trends pre-2010 of 0.99−2.28 $\mu g/m^3$/year, but are approximately neutral post-2010. South Asia is now the region with the highest $PM_{2.5}$. North America has shifted from a clear summertime maximum to similar summer and winter $PM_{2.5}$ concentrations over this time period, reflecting in part regional implementation of sulfur-emission reduction technologies[54] and reductions in summertime organic aerosol in the Southeast United States.[55]

Figure 4 shows the mean monthly population-weighted $PM_{2.5}$ variation by the GBD region over the past decade. Supporting Information Table S4 summarizes the month of maximum and minimum $PM_{2.5}$ exposure, as well as annual mean $PM_{2.5}$ exposure over these regions. Seasonal variations can be large, such as the wintertime maxima over East Asia, South Asia, and Central Europe, which exceed corresponding summertime minima by a factor of 2−3. South Asia, for example, has a January maximum $PM_{2.5}$ of 93 $\mu g/m^3$ and an August minimum of 34 $\mu g/m^3$. This variation is less pronounced over Western and Eastern Europe, although these regions still have seasonal wintertime enhancements of 50−100%. Seasonal maxima in developing regions, such as Latin America and Africa, are often influenced by mineral dust or biomass burning emissions.[56,57]

Figure 5 shows monthly Apte plots[58] of the regional distributions of population versus $PM_{2.5}$ for 2018, providing further insight into the broad seasonal shifts (Figure 4). In January, $PM_{2.5}$ concentrations exhibit pronounced regional variability of nearly two orders of magnitude. Subregional heterogeneity within South Asia has a large segment of that population exposed to about 50 $\mu g/m^3$ in January, but with a distinct peak of ∼200 $\mu g/m^3$ corresponding to populations within the Ganga basin and Bangladesh.

Figure 6 shows the predicted monthly per-pixel hybrid $PM_{2.5}$ uncertainty ($PM_{2.5}{}'_{hyb}$) for January, April, July, and October 2018. Individual contributions to this uncertainty are shown in Supporting Information Figure S7. Higher absolute uncertainty levels generally correspond to higher $PM_{2.5}$ concentrations, such as over areas with large-scale biomass burning and mineral dust features that present challenging conditions for both AOD retrieval and η representation. Over densely

https://doi.org/10.1021/acs.est.1c05309
Environ. Sci. Technol. 2021, 55, 15287−15300

Table 2. Comparison of Monthly Geometric Mean Hybrid ($PM_{2.5}'_{hyb}$) and Observed ($PM_{2.5}'_{obs}$) Uncertainties by the Sample Averaging Size and the GBD Region, 2015−2019, in $\mu g/m^3$[a]

GBD region	type of $PM_{2.5}'$	January						July						no. of monitors
		geo. mean $PM_{2.5}$	geo. mean $PM_{2.5}'N=$ 1	10	50	100	500	geo. mean $PM_{2.5}$	geo. mean $PM_{2.5}'N=$ 1	10	50	100	500	
global	hyb	20	6.2	1.9	0.9	0.6	0.3	14	4.4	1.4	0.6	0.4	0.2	11,015
	obs	20	5.3	2.2	1.2	0.9	0.6	14	3.3	1.4	0.7	0.6	0.4	
Asia Pacific, high income	hyb	16	4.3	1.4	0.6	0.4		16	5.3	1.7	0.7	0.5		181
	obs	16	3.3	1.5	0.6	0.5		15	2.6	1.2	0.6	0.5		
Asia, Central	hyb	40	7.9	2.8				19	5.0	1.6				29
	obs	33	32	12				16	13	6.1				
Asia, East	hyb	61	14	4.6	2.0	1.4	0.6	27	7.3	2.3	1.0	0.7	0.3	2879
	obs	62	10	4.5	2.6	2.0	1.5	27	4.9	2.0	1.0	0.8	0.4	
Asia, South	hyb	69	22	6.9	3.1	2.2		31	9.4	3.0	1.3	0.9		367
	obs	66	30	11	6.0	4.4		29	13	5.2	3.6	3.1		
Asia, Southeast	hyb	27	8.1	2.5	1.1	0.8		20	7.2	2.2	1.0	0.7		145
	obs	26	12	4.6	1.8	1.1		19	12	4.7	2.0	1.5		
Australasia	hyb	7.1	2.7	0.9	0.4	0.3		7.2	2.3	0.7	0.3	0.2		202
	obs	6.9	1.9	0.7	0.3	0.2		7.6	1.9	0.8	0.5	0.4		
Caribbean	hyb	18	14	4.6				22	30	9.3				26
	obs	18	5.6	2.4				21	8.9	3.6				
Europe, Central	hyb	31	6.7	2.1	0.9	0.7	0.3	12	3.1	1.0	0.4	0.3	0.1	759
	obs	30	8.3	3.0	1.5	1.2	0.8	12	3.1	1.2	0.7	0.6	0.5	
Europe, Eastern	hyb	11	4.8	1.5	0.7			9.1	3.1	1.0	0.4			89
	obs	9.6	5.8	2.5	1.7			8.7	3.6	1.4	0.6			
Europe, Western	hyb	15	3.9	1.2	0.6	0.4	0.2	10.0	2.9	0.9	0.4	0.3	0.1	2533
	obs	14	3.4	1.4	0.8	0.7	0.6	9.7	2.4	0.9	0.5	0.5	0.4	
Latin America, Andean	hyb	19	11	3.4				24	14	4.4				47
	obs	19	8.3	2.3				23	12	3.4				
Latin America, Central	hyb	23	9.1	2.9	1.3	0.9		18	8.8	2.9	1.2	0.9		162
	obs	23	6.8	2.4	0.9	0.6		18	4.8	1.8	0.8	0.5		
Latin America, Southern	hyb	14	8.5	2.7	1.2	0.8		26	11	3.4	1.5	1.1		111
	obs	13	7.5	2.8	1.6	1.5		26	9.6	4.2	1.5	0.8		
Latin America, Tropical	hyb	12	5.3	1.7	0.8	0.5		16	7.3	2.3	1.0	0.7		161
	obs	12	3.7	1.6	1.1	1.0		16	4.6	1.8	0.8	0.5		
North Africa/Middle East	hyb	33	8.4	2.6	1.2	0.8		32	8.8	2.7	1.2	0.9		309
	obs	35	14	5.4	3.1	2.8		33	13	4.6	2.0	1.5		
North America, high income	hyb	7.2	3.2	1.0	0.5	0.3	0.1	7.7	3.1	1.0	0.5	0.3	0.1	2900
	obs	6.8	1.9	1.0	0.6	0.5	0.5	7.5	1.8	0.7	0.4	0.3	0.3	
Sub-Saharan Africa, southern	hyb	33	20	6.5				30	20	6.5				49
	obs	30	18	6.3				32	16	5.2				
Sub-Saharan Africa, west	hyb	57	30	9.6				27	7.6	2.5				32
	obs	55	29	8.3				23	15	6.3				

[a] $PM_{2.5}'_{obs}$ is represented using the 68th percentile of differences between the observed and cross-validated hybrid $PM_{2.5}$. Sample averaging size, N, represents the number of sites agglomerated prior to uncertainty comparison, where agglomeration sites are selected randomly within each corresponding GBD region. Agglomerated $PM_{2.5}'_{hyb}$ are scaled by $N^{-1/2}$, assuming random errors. Geometric mean $PM_{2.5}$ concentrations are also given for all sites within each region. Values are collocated with ground-based monitors and not representative of the overall regional means. Only regions with at least 10 ground-based monitors are included.

monitored regions, stronger constraints for GWR parameters are demonstrated by relatively low $PM_{2.5}'_{GWR}$, whereas $PM_{2.5}'_{AOD}$ follows the magnitude of AOD itself or challenging retrieval conditions. Percentage-wise, uncertainty levels are generally the highest where $PM_{2.5}$ concentrations are low such as remote northern regions and the Tibetan Plateau (Supporting Information, Figure S8). The overall monthly per-pixel (1 km × 1 km) uncertainties of around 20% are estimated for the most heavily populated regions of East Asia and South Asia and 30−50% over North America.

Table 2 compares $PM_{2.5}'_{hyb}$ with the observed uncertainty ($PM_{2.5}'_{obs}$), as represented by differences between ground-based and hybrid $PM_{2.5}$. Regional consistency is found between $PM_{2.5}'_{hyb}$ and $PM_{2.5}'_{obs}$, with the largest uncertainties found over the relatively under-monitored regions of Africa, Latin America, and Asia. The observed agglomerated and hybrid $PM_{2.5}$ prior to the calculation of $PM_{2.5}'_{obs}$ greatly reduce this uncertainty across all regions. Similar decreases are found by scaling the agglomerated $PM_{2.5}'_{hyb}$ by $N^{-1/2}$, suggesting a large random component to hybrid $PM_{2.5}$ uncertainties, and implying a method to represent regional hybrid $PM_{2.5}$ uncertainties. This representation will permit future studies to directly explore the impact of hybrid $PM_{2.5}$ uncertainties on health-impact assessments and epidemiological analysis, as well as demonstrates the robustness of hybrid $PM_{2.5}$ for estimates at regional scales.

https://doi.org/10.1021/acs.est.1c05309
Environ. Sci. Technol. 2021, 55, 15287−15300

In summary, the pronounced seasonal variation revealed by monthly global satellite-derived $PM_{2.5}$ concentrations identifies a broad pattern of elevated $PM_{2.5}$ concentrations in densely populated regions of South Asia, East Asia, and Eastern Europe in winter, which may provide insight into measures that would reduce the overall $PM_{2.5}$ exposure. Additionally, it is anticipated that these data will enable further study into associations and burdens of $PM_{2.5}$ on window-dependent health effects, such as in-utero infant development. Novel quantification of per-pixel uncertainty offers information to aid the interpretation of monthly $PM_{2.5}$ data and the significance of related findings.

The hybrid $PM_{2.5}$ and uncertainty estimates presented in this work are freely available as a public good via the Washington University Atmospheric Composition Analysis Group website as version V5.GL.01 at https://sites.wustl.edu/acag/datasets/surface-pm2-5/ or by contacting the authors.

■ ASSOCIATED CONTENT

Supporting Information

The Supporting Information is available free of charge at https://pubs.acs.org/doi/10.1021/acs.est.1c05309.

Monthly global estimates of fine particulate matter and their uncertainty supporting information (PDF)

■ AUTHOR INFORMATION

Corresponding Author

Aaron van Donkelaar − *Department of Energy, Environmental, and Chemical Engineering, Washington University in St. Louis, St. Louis, Missouri 63130, United States; Department of Physics and Atmospheric Science, Dalhousie University, Halifax, Nova Scotia B3H 3J5, Canada;* orcid.org/0000-0002-2998-8521; Email: aaron.vandonkelaar@wustl.edu

Authors

Melanie S. Hammer − *Department of Energy, Environmental, and Chemical Engineering, Washington University in St. Louis, St. Louis, Missouri 63130, United States;* orcid.org/0000-0001-8443-7979

Liam Bindle − *Department of Energy, Environmental, and Chemical Engineering, Washington University in St. Louis, St. Louis, Missouri 63130, United States*

Michael Brauer − *School of Population and Public Health, University of British Columbia, Vancouver, British Columbia V6T 1Z3, Canada; Institute for Health Metrics and Evaluation, University of Washington, Seattle, Washington 98195, United States;* orcid.org/0000-0002-9103-9343

Jeffery R. Brook − *Dalla Lana School of Public Health, University of Toronto, Toronto, Ontario M5T 1P8, Canada*

Michael J. Garay − *Jet Propulsion Laboratory, California Institute of Technology, Pasadena, California 91109, United States*

N. Christina Hsu − *Earth Sciences Division, NASA Goddard Space Flight Center, Greenbelt, Maryland 20771, United States*

Olga V. Kalashnikova − *Jet Propulsion Laboratory, California Institute of Technology, Pasadena, California 91109, United States*

Ralph A. Kahn − *Earth Sciences Division, NASA Goddard Space Flight Center, Greenbelt, Maryland 20771, United States*

Colin Lee − *Department of Physics and Atmospheric Science, Dalhousie University, Halifax, Nova Scotia B3H 3J5, Canada*

Robert C. Levy − *Earth Sciences Division, NASA Goddard Space Flight Center, Greenbelt, Maryland 20771, United States*

Alexei Lyapustin − *Earth Sciences Division, NASA Goddard Space Flight Center, Greenbelt, Maryland 20771, United States*

Andrew M. Sayer − *Earth Sciences Division, NASA Goddard Space Flight Center, Greenbelt, Maryland 20771, United States; Goddard Earth Sciences Technology and Research, Universities Space Research Association, Columbia, Maryland 21046, United States*

Randall V. Martin − *Department of Energy, Environmental, and Chemical Engineering, Washington University in St. Louis, St. Louis, Missouri 63130, United States; Department of Physics and Atmospheric Science, Dalhousie University, Halifax, Nova Scotia B3H 3J5, Canada*

Complete contact information is available at: https://pubs.acs.org/10.1021/acs.est.1c05309

Notes

The authors declare no competing financial interest.

■ ACKNOWLEDGMENTS

We are grateful to the MODIS, MISR, SeaWiFS, and AERONET teams that have made this work possible through the creation, validation, and public release of their data products, as well as the support provided by the Canadian Urban Environmental Health Research Consortium, by the Natural Science and Engineering Council of Canada (RGPIN-2019-04670), by Washington University, by the John D. and Catherine T. MacAuthor Foundation, and by the NASA Applied Sciences Program (Grant Number 80NSSC21K0508).

■ REFERENCES

(1) Murray, C. J. L.; Aravkin, A. Y.; Zheng, P.; Abbafati, C.; Abbas, K. M.; Abbasi-Kangevari, M.; Abd-Allah, F.; Abdelalim, A.; Abdollahi, M.; Abdollahpour, I.; Abegaz, K. H.; Abolhassani, H.; Aboyans, V.; Abreu, L. G.; Abrigo, M. R. M.; Abualhasan, A.; Abu-Raddad, L. J.; Abushouk, A. I.; Adabi, M.; Adekanmbi, V.; Adeoye, A. M.; Adetokunboh, O. O.; Adham, D.; Advani, S. M.; Agarwal, G.; Aghamir, S. M. K.; Agrawal, A.; Ahmad, T.; Ahmadi, K.; Ahmadi, M.; Ahmadieh, H.; Ahmed, M. B.; Akalu, T. Y.; Akinyemi, R. O.; Akinyemiju, T.; Akombi, B.; Akunna, C. J.; Alahdab, F.; Al-Aly, Z.; Alam, K.; Alam, S.; Alam, T.; Alanezi, F. M.; Alanzi, T. M.; Alemu, B. W.; Alhabib, K. F.; Ali, M.; Ali, S.; Alicandro, G.; Alinia, C.; Alipour, V.; Alizade, H.; Aljunid, S. M.; Alla, F.; Allebeck, P.; Almasi-Hashiani, A.; Al-Mekhlafi, H. M.; Alonso, J.; Altirkawi, K. A.; Amini-Rarani, M.; Amiri, F.; Amugsi, D. A.; Ancuceanu, R.; Anderlini, D.; Anderson, J. A.; Andrei, C. L.; Andrei, T.; Angus, C.; Anjomshoa, M.; Ansari, F.; Ansari-Moghaddam, A.; Antonazzo, I. C.; Antonio, C. A. T.; Antony, C. M.; Antriyandarti, E.; Anvari, D.; Anwer, R.; Appiah, S. C. Y.; Arabloo, J.; Arab-Zozani, M.; Ariani, F.; Armoon, B.; Ärnlöv, J.; Arzani, A.; Asadi-Aliabadi, M.; Asadi-Pooya, A. A.; Ashbaugh, C.; Assmus, M.; Atafar, Z.; Atnafu, D. D.; Atout, M. M. D. W.; Ausloos, F.; Ausloos, M.; Ayala Quintanilla, B. P.; Ayano, G.; Ayanore, M. A.; Azari, S.; Azarian, G.; Azene, Z. N.; Badawi, A.; Badiye, A. D.; Bahrami, M. A.; Bakhshaei, M. H.; Bakhtiari, A.; Bakkannavar, S. M.; Baldasseroni, A.; Ball, K.; Ballew, S. H.; Balzi, D.; Banach, M.; Banerjee, S. K.; Bante, A. B.; Baraki, A. G.; Barker-Collo, S. L.; Bärnighausen, T. W.; Barrero, L. H.; Barthelemy, C. M.; Barua, L.; Basu, S.; Baune, B. T.; Bayati, M.; Becker, J. S.; Bedi, N.; Beghi, E.; Béjot, Y.; Bell, M. L.; Bennitt, F. B.; Bensenor, I. M.; Berhe, K.;

Berman, A. E.; Bhagavathula, A. S.; Bhageerathy, R.; Bhala, N.; Bhandari, D.; Bhattacharyya, K.; Bhutta, Z. A.; Bijani, A.; Bikbov, B.; Bin Sayeed, M. S.; Biondi, A.; Birihane, B. M.; Bisignano, C.; Biswas, R. K.; Bitew, H.; Bohlouli, S.; Bohluli, M.; Boon-Dooley, A. S.; Borges, G.; Borzì, A. M.; Borzouei, S.; Bosetti, C.; Boufous, S.; Braithwaite, D.; Breitborde, N. J. K.; Breitner, S.; Brenner, H.; Briant, P. S.; Briko, A. N.; Briko, N. I.; Britton, G. B.; Bryazka, D.; Bumgarner, B. R.; Burkart, K.; Burnett, R. T.; Burugina Nagaraja, S.; Butt, Z. A.; Caetano dos Santos, F. L.; Cahill, L. E.; Cámera, L. L. A. A.; Campos-Nonato, I. R.; Cárdenas, R.; Carreras, G.; Carrero, J. J.; Carvalho, F.; Castaldelli-Maia, J. M.; Castañeda-Orjuela, C. A.; Castelpietra, G.; Castro, F.; Causey, K.; Cederroth, C. R.; Cercy, K. M.; Cerin, E.; Chandan, J. S.; Chang, K.-L.; Charlson, F. J.; Chattu, V. K.; Chaturvedi, S.; Cherbuin, N.; Chimed-Ochir, O.; Cho, D. Y.; Choi, J.-Y. J.; Christensen, H.; Chu, D.-T.; Chung, M. T.; Chung, S.-C.; Cicuttini, F. M.; Ciobanu, L. G.; Cirillo, M.; Classen, T. K. D.; Cohen, A. J.; Compton, K.; Cooper, O. R.; Costa, V. M.; Cousin, E.; Cowden, R. G.; Cross, D. H.; Cruz, J. A.; Dahlawi, S. M. A.; Damasceno, A. A. M.; Damiani, G.; Dandona, L.; Dandona, R.; Dangel, W. J.; Danielsson, A.-K.; Dargan, P. I.; Darwesh, A. M.; Daryani, A.; Das, J. K.; Das Gupta, R.; das Neves, J.; Dávila-Cervantes, C. A.; Davitoiu, D. V.; De Leo, D.; Degenhardt, L.; DeLang, M.; Dellavalle, R. P.; Demeke, F. M.; Demoz, G. T.; Demsie, D. G.; Denova-Gutiérrez, E.; Dervenis, N.; Dhungana, G. P.; Dianatinasab, M.; Dias da Silva, D.; Diaz, D.; Dibaji Forooshani, Z. S.; Djalalinia, S.; Do, H. T.; Dokova, K.; Dorostkar, F.; Doshmangir, L.; Driscoll, T. R.; Duncan, B. B.; Duraes, A. R.; Eagan, A. W.; Edvardsson, D.; El Nahas, N.; El Sayed, I.; El Tantawi, M.; Elbarazi, I.; Elgendy, I. Y.; El-Jaafary, S. I.; Elyazar, I. R. F.; Emmons-Bell, S.; Erskine, H. E.; Eskandarieh, S.; Esmaeilnejad, S.; Esteghamati, A.; Estep, K.; Etemadi, A.; Etisso, A. E.; Fanzo, J.; Farahmand, M.; Fareed, M.; Faridnia, R.; Farioli, A.; Faro, A.; Faruque, M.; Farzadfar, F.; Fattahi, N.; Fazlzadeh, M.; Feigin, V. L.; Feldman, R.; Fereshtehnejad, S.-M.; Fernandes, E.; Ferrara, G.; Ferrari, A. J.; Ferreira, M. L.; Filip, I.; Fischer, F.; Fisher, J. L.; Flor, L. S.; Foigt, N. A.; Folayan, M. O.; Fomenkov, A. A.; Force, L. M.; Foroutan, M.; Franklin, R. C.; Freitas, M.; Fu, W.; Fukumoto, T.; Furtado, J. M.; Gad, M. M.; Gakidou, E.; Gallus, S.; Garcia-Basteiro, A. L.; Gardner, W. M.; Geberemariyam, B. S.; Gebreslassie, A. A. A. A.; Geremew, A.; Gershberg Hayoon, A.; Gething, P. W.; Ghadimi, M.; Ghadiri, K.; Ghaffarifar, F.; Ghafourifard, M.; Ghamari, F.; Ghashghaee, A.; Ghiasvand, H.; Ghith, N.; Gholamian, A.; Ghosh, R.; Gill, P. S.; Ginindza, T. G. G.; Giussani, G.; Gnedovskaya, E. V.; Goharinezhad, S.; Gopalani, S. V.; Gorini, G.; Goudarzi, H.; Goulart, A. C.; Greaves, F.; Grivna, M.; Grosso, G.; Gubari, M. I. M.; Gugnani, H. C.; Guimarães, R. A.; Guled, R. A.; Guo, G.; Guo, Y.; Gupta, R.; Gupta, T.; Haddock, B.; Hafezi-Nejad, N.; Hafiz, A.; Haj-Mirzaian, A.; Haj-Mirzaian, A.; Hall, B. J.; Halvaei, I.; Hamadeh, R. R.; Hamidi, S.; Hammer, M. S.; Hankey, G. J.; Haririan, H.; Haro, J. M.; Hasaballah, A. I.; Hasan, M. M.; Hasanpoor, E.; Hashi, A.; Hassanipour, S.; Hassankhani, H.; Havmoeller, R. J.; Hay, S. I.; Hayat, K.; Heidari, G.; Heidari-Soureshjani, R.; Henrikson, H. J.; Herbert, M. E.; Herteliu, C.; Heydarpour, F.; Hird, T. R.; Hoek, H. W.; Holla, R.; Hoogar, P.; Hosgood, H. D.; Hossain, N.; Hosseini, M.; Hosseinzadeh, M.; Hostiuc, M.; Hostiuc, S.; Househ, M.; Hsairi, M.; Hsieh, V. C.-R.; Hu, G.; Hu, K.; Huda, T. M.; Humayun, A.; Huynh, C. K.; Hwang, B.-F.; Iannucci, V. C.; Ibitoye, S. E.; Ikeda, N.; Ikuta, K. S.; Ilesanmi, O. S.; Ilic, I. M.; Ilic, M. D.; Inbaraj, L. R.; Ippolito, H.; Iqbal, U.; Irvani, S. S. N.; Irvine, C. M. S.; Islam, M. M.; Islam, S. M. S.; Iso, H.; Ivers, R. Q.; Iwu, C. C. D.; Iwu, C. J.; Iyamu, I. O.; Jaafari, J.; Jacobsen, K. H.; Jafari, H.; Jafarinia, M.; Jahani, M. A.; Jakovljevic, M.; Jalilian, F.; James, S. L.; Janjani, H.; Javaheri, T.; Javidnia, J.; Jeemon, P.; Jenabi, E.; Jha, R. P.; Jha, V.; Ji, J. S.; Johansson, L.; John, O.; John-Akinola, Y. O.; Johnson, C. O.; Jonas, J. B.; Joukar, F.; Jozwiak, J. J.; Jürisson, M.; Kabir, A.; Kabir, Z.; Kalani, H.; Kalani, R.; Kalankesh, L. R.; Kalhor, R.; Kanchan, T.; Kapoor, N.; Karami Matin, B.; Karch, A.; Karim, M. A.; Kassa, G. M.; Katikireddi, S. V.; Kayode, G. A.; Kazemi Karyani, A.; Keiyoro, P. N.; Keller, C.; Kemmer, L.; Kendrick, P. J.; Khalid, N.; Khammarnia, M.; Khan, E. A.; Khan, M.; Khatab, K.; Khater, M. M.; Khatib, M. N.; Khayamzadeh, M.; Khazaei, S.; Kieling, C.; Kim, Y. J.; Kimokoti, R. W.; Kisa, A.; Kisa, S.; Kivimäki, M.; Knibbs, L. D.; Knudsen, A. K. S.; Kocarnik, J. M.; Kochhar, S.; Kopec, J. A.; Korshunov, V. A.; Koul, P. A.; Koyanagi, A.; Kraemer, M. U. G.; Krishan, K.; Krohn, K. J.; Kromhout, H.; Kuate Defo, B.; Kumar, G. A.; Kumar, V.; Kurmi, O. P.; Kusuma, D.; La Vecchia, C.; Lacey, B.; Lal, D. K.; Lalloo, R.; Lallukka, T.; Lami, F. H.; Landires, I.; Lang, J. J.; Langan, S. M.; Larsson, A. O.; Lasrado, S.; Lauriola, P.; Lazarus, J. V.; Lee, P. H.; Lee, S. W. H.; LeGrand, K. E.; Leigh, J.; Leonardi, M.; Lescinsky, H.; Leung, J.; Levi, M.; Li, S.; Lim, L.-L.; Linn, S.; Liu, S.; Liu, S.; Liu, Y.; Lo, J.; Lopez, A. D.; Lopez, J. C. F.; Lopukhov, P. D.; Lorkowski, S.; Lotufo, P. A.; Lu, A.; Lugo, A.; Maddison, E. R.; Mahasha, P. W.; Mahdavi, M. M.; Mahmoudi, M.; Majeed, A.; Maleki, A.; Maleki, S.; Malekzadeh, R.; Malta, D. C.; Mamun, A. A.; Manda, A. L.; Manguerra, H.; Mansour-Ghanaei, F.; Mansouri, B.; Mansournia, M. A.; Mantilla Herrera, A. M.; Maravilla, J. C.; Marks, A.; Martin, R. V.; Martini, S.; Martins-Melo, F. R.; Masaka, A.; Masoumi, S. Z.; Mathur, M. R.; Matsushita, K.; Maulik, P. K.; McAlinden, C.; McGrath, J. J.; McKee, M.; Mehndiratta, M. M.; Mehri, F.; Mehta, K. M.; Memish, Z. A.; Mendoza, W.; Menezes, R. G.; Mengesha, E. W.; Mereke, A.; Mereta, S. T.; Meretoja, A.; Meretoja, T. J.; Mestrovic, T.; Miazgowski, B.; Miazgowski, T.; Michalek, I. M.; Miller, T. R.; Mills, E. J.; Mini, G. K.; Miri, M.; Mirica, A.; Mirrakhimov, E. M.; Mirzaei, H.; Mirzaei, M.; Mirzaei, R.; Mirzaei-Alavijeh, M.; Misganaw, A. T.; Mithra, P.; Moazen, B.; Mohammad, D. K.; Mohammad, Y.; Mohammad Gholi Mezerji, N.; Mohammadian-Hafshejani, A.; Mohammadifard, N.; Mohammadpourhodki, R.; Mohammed, A. S.; Mohammed, H.; Mohammed, J. A.; Mohammed, S.; Mokdad, A. H.; Molokhia, M.; Monasta, L.; Mooney, M. D.; Moradi, G.; Moradi, M.; Moradi-Lakeh, M.; Moradzadeh, R.; Moraga, P.; Morawska, L.; Morgado-da-Costa, J.; Morrison, S. D.; Mosapour, A.; Mosser, J. F.; Mouodi, S.; Mousavi, S. M.; Mousavi Khaneghah, A.; Mueller, U. O.; Mukhopadhyay, S.; Mullany, E. C.; Musa, K. I.; Muthupandian, S.; Nabhan, A. F.; Naderi, M.; Nagarajan, A. J.; Nagel, G.; Naghavi, M.; Naghshtabrizi, B.; Naimzada, M. D.; Najafi, F.; Nangia, V.; Nansseu, J. R.; Naserbakht, M.; Nayak, V. C.; Negoi, I.; Ngunjiri, J. W.; Nguyen, C. T.; Nguyen, H. L. T.; Nguyen, M.; Nigatu, Y. T.; Nikbakhsh, R.; Nixon, M. R.; Nnaji, C. A.; Nomura, S.; Norrving, B.; Noubiap, J. J.; Nowak, C.; Nunez-Samudio, V.; Oţoiu, A.; Oancea, B.; Odell, C. M.; Ogbo, F. A.; Oh, I.-H.; Okunga, E. W.; Oladnabi, M.; Olagunju, A. T.; Olusanya, B. O.; Olusanya, J. O.; Omer, M. O.; Ong, K. L.; Onwujekwe, O. E.; Orpana, H. M.; Ortiz, A.; Osarenotor, O.; Osei, F. B.; Ostroff, S. M.; Otstavnov, N.; Otstavnov, S. S.; Øverland, S.; Owolabi, M. O.; Padubidri, J. R.; Palladino, R.; Panda-Jonas, S.; Pandey, A.; Parry, C. D. H.; Pasovic, M.; Pasupula, D. K.; Patel, S. K.; Pathak, M.; Patten, S. B.; Patton, G. C.; Pazoki Toroudi, H.; Peden, A. E.; Pennini, A.; Pepito, V. C. F.; Peprah, E. K.; Pereira, D. M.; Pesudovs, K.; Pham, H. Q.; Phillips, M. R.; Piccinelli, C.; Pilz, T. M.; Piradov, M. A.; Pirsaheb, M.; Plass, D.; Polinder, S.; Polkinghorne, K. R.; Pond, C. D.; Postma, M. J.; Pourjafar, H.; Pourmalek, F.; Poznańska, A.; Prada, S. I.; Prakash, V.; Pribadi, D. R. A.; Pupillo, E.; Quazi Syed, Z.; Rabiee, M.; Rabiee, N.; Radfar, A.; Rafiee, A.; Raggi, A.; Rahman, M. A.; Rajabpour-Sanati, A.; Rajati, F.; Rakovac, I.; Ram, P.; Ramezanzadeh, K.; Ranabhat, C. L.; Rao, P. C.; Rao, S. J.; Rashedi, V.; Rathi, P.; Rawaf, D. L.; Rawaf, S.; Rawal, L.; Rawassizadeh, R.; Rawat, R.; Razo, C.; Redford, S. B.; Reiner, R. C.; Reitsma, M. B.; Remuzzi, G.; Renjith, V.; Renzaho, A. M. N.; Resnikoff, S.; Rezaei, N.; Rezaei, N.; Rezapour, A.; Rhinehart, P.-A.; Riahi, S. M.; Ribeiro, D. C.; Ribeiro, D.; Rickard, J.; Rivera, J. A.; Roberts, N. L. S.; Rodríguez-Ramírez, S.; Roever, L.; Ronfani, L.; Room, R.; Roshandel, G. A.; Roth, G. A.; Rothenbacher, D.; Rubagotti, E.; Rwegerera, G. M.; Sabour, S.; Sachdev, P. S.; Saddik, B.; Sadeghi, E.; Sadeghi, M.; Saeedi, R.; Saeedi, M. S.; Safari, Y.; Safi, S.; Safiri, S.; Sagar, R.; Sahebkar, A.; Sajadi, S. M.; Salam, N.; Salamati, P.; Salem, H.; Salem, M. R. R.; Salimzadeh, H.; Salman, O. M.; Salomon, J. A.; Samad, Z.; Samadi Kafil, H.; Sambala, E. Z.; Samy, A. M.; Sanabria, J.; Sánchez-Pimienta, T. G.; Santomauro, D. F.; Santos, I. S.; Santos, J. V.; Santric-Milicevic, M. M.; Saraswathy, S. Y. I.; Sarmiento-Suárez, R.; Sarrafzadegan, N.; Sartorius, B.; Sarveazad, A.; Sathian, B.; Sathish, T.; Sattin, D.; Saxena,

https://doi.org/10.1021/acs.est.1c05309
Environ. Sci. Technol. 2021, 55, 15287−15300

S.; Schaeffer, L. E.; Schiavolin, S.; Schlaich, M. P.; Schmidt, M. I.; Schutte, A. E.; Schwebel, D. C.; Schwendicke, F.; Senbeta, A. M.; Senthilkumaran, S.; Sepanlou, S. G.; Serdar, B.; Serre, M. L.; Shadid, J.; Shafaat, O.; Shahabi, S.; Shaheen, A. A.; Shaikh, M. A.; Shalash, A. S.; Shams-Beyranvand, M.; Shamsizadeh, M.; Sharafi, K.; Sheikh, A.; Sheikhtaheri, A.; Shibuya, K.; Shield, K. D.; Shigematsu, M.; Shin, J. I.; Shin, M.-J.; Shiri, R.; Shirkoohi, R.; Shuval, K.; Siabani, S.; Sierpinski, R.; Sigfusdottir, I. D.; Sigurvinsdottir, R.; Silva, J. P.; Simpson, K. E.; Singh, J. A.; Singh, P.; Skiadaresi, E.; Skou, S. T. S.; Skryabin, V. Y.; Smith, E. U. R.; Soheili, A.; Soltani, S.; Soofi, M.; Sorensen, R. J. D.; Soriano, J. B.; Sorrie, M. B.; Soshnikov, S.; Soyiri, I. N.; Spencer, C. N.; Spotin, A.; Sreeramareddy, C. T.; Srinivasan, V.; Stanaway, J. D.; Stein, C.; Stein, D. J.; Steiner, C.; Stockfelt, L.; Stokes, M. A.; Straif, K.; Stubbs, J. L.; Sufiyan, M. A. B.; Suleria, H. A. R.; Suliankatchi, A. R.; Sulo, G.; Sultan, I.; Szumowski, Ł.; Tabarés-Seisdedos, R.; Tabb, K. M.; Tabuchi, T.; Taherkhani, A.; Tajdini, M.; Takahashi, K.; Takala, J. S.; Tamiru, A. T.; Taveira, N.; Tehrani-Banihashemi, A.; Temsah, M.-H.; Tesema, G. A.; Tessema, Z. T.; Thurston, G. D.; Titova, M. V.; Tohidinik, H. R.; Tonelli, M.; Topor-Madry, R.; Topouzis, F.; Torre, A. E.; Touvier, M.; Tovani-Palone, M. R. R.; Tran, B. X.; Travillian, R.; Tsatsakis, A.; Tudor Car, L.; Tyrovolas, S.; Uddin, R.; Umeokonkwo, C. D.; Unnikrishnan, B.; Upadhyay, E.; Vacante, M.; Valdez, P. R.; van Donkelaar, A.; Vasankari, T. J.; Vasseghian, Y.; Veisani, Y.; Venketasubramanian, N.; Violante, F. S.; Vlassov, V.; Vollset, S. E.; Vos, T.; Vukovic, R.; Waheed, Y.; Wallin, M. T.; Wang, Y.; Wang, Y.-P.; Watson, A.; Wei, J.; Wei, M. Y. W.; Weintraub, R. G.; Weiss, J.; Werdecker, A.; West, J. J.; Westerman, R.; Whisnant, J. L.; Whiteford, H. A.; Wiens, K. E.; Wolfe, C. D. A.; Wozniak, S. S.; Wu, A.-M.; Wu, J.; Wulf Hanson, S.; Xu, G.; Xu, R.; Yadgir, S.; Yahyazadeh Jabbari, S. H.; Yamagishi, K.; Yaminfirooz, M.; Yano, Y.; Yaya, S.; Yazdi-Feyzabadi, V.; Yeheyis, T. Y.; Yilgwan, C. S.; Yilma, M. T.; Yip, P.; Yonemoto, N.; Younis, M. Z.; Younker, T. P.; Yousefi, B.; Yousefi, Z.; Yousefinezhadi, T.; Yousuf, A. Y.; Yu, C.; Yusefzadeh, H.; Zahirian Moghadam, T.; Zamani, M.; Zamanian, M.; Zandian, H.; Zastrozhin, M. S.; Zhang, Y.; Zhang, Z.-J.; Zhao, J. T.; Zhao, X.-J. G.; Zhao, Y.; Zhou, M.; Ziapour, A.; Zimsen, S. R. M.; Brauer, M.; Afshin, A.; Lim, S. S. Global burden of 87 risk factors in 204 countries and territories, 1990−2019: a systematic analysis for the Global Burden of Disease Study 2019. *Lancet* **2020**, *396*, 1223−1249.

(2) Martin, R. V.; Brauer, M.; van Donkelaar, A.; Shaddick, G.; Narain, U.; Dey, S. No one knows which city has the highest concentration of fine particulate matter. *Atmos. Environ.: X* **2019**, *3*, No. 100040.

(3) Hammer, M. S.; van Donkelaar, A.; Li, C.; Lyapustin, A.; Sayer, A. M.; Hsu, N. C.; Levy, R. C.; Garay, M.; Kalashnikova, O.; Kahn, R. A.; Brauer, M.; Apte, J. S.; Henze, D. K.; Zhang, L.; Zhang, Q.; Ford, B.; Pierce, J. R.; Martin, R. V. Global Estimates and Long-Term Trends of Fine Particulate Matter Concentrations (1998-2018). *Environ. Sci. Technol.* **2020**, *54*, 7879−7890.

(4) Shaddick, G.; Thomas, M.; Amini, H.; Broday, D.; Cohen, A.; Frostad, J.; Green, A.; Gumy, S.; Liu, Y.; Martin, R.; Pruss-Ustun, A.; Simpson, D.; van Donkelaar, A.; Brauer, M. Data Integration for the Assessment of Population Exposure to Ambient Air Pollution for Global Burden of Disease Assessment. *Environ. Sci. Technol.* **2018**, *52*, 9069−9078.

(5) van Donkelaar, A.; Martin, R. V.; Li, C.; Burnett, R. T. Regional Estimates of Chemical Composition of Fine Particulate Matter Using a Combined Geoscience-Statistical Method with Information from Satellites, Models, and Monitors. *Environ. Sci. Technol.* **2019**, *53*, 2595.

(6) Huang, C.; Hu, J.; Xue, T.; Xu, H.; Wang, M. High-Resolution Spatiotemporal Modeling for Ambient PM2.5 Exposure Assessment in China from 2013 to 2019. *Environ. Sci. Technol.* **2021**, *55*, 2152−2162.

(7) Di, Q.; Amini, H.; Shi, L.; Kloog, I.; Silvern, R.; Kelly, J.; Sabath, M. B.; Choirat, C.; Koutrakis, P.; Lyapustin, A.; Wang, Y.; Mickley, L. J.; Schwartz, J. An ensemble-based model of PM2.5 concentration across the contiguous United States with high spatiotemporal resolution. *Environ. Int.* **2019**, *130*, No. 104909.

(8) Hu, X.; Belle, J. H.; Meng, X.; Wildani, A.; Waller, L. A.; Strickland, M. J.; Liu, Y. Estimating PM2.5 Concentrations in the Conterminous United States Using the Random Forest Approach. *Environ. Sci. Technol.* **2017**, *51*, 6936−6944.

(9) van Donkelaar, A.; Martin, R. V.; Spurr, R. J. D.; Burnett, R. T. High-resolution satellite-derived $PM_{2.5}$ from optimal estimation and geographically weighted regression over North America. *Environ. Sci. Technol.* **2015**, *49*, 10482−10491.

(10) Bai, L.; Shin, S.; Burnett, R. T.; Kwong, J. C.; Hystad, P.; van Donkelaar, A.; Goldberg, M. S.; Lavigne, E.; Copes, R.; Martin, R. V.; Kopp, A.; Chen, H. Exposure to ambient air pollution and the incidence of congestive heart failure and acute myocardial infarction: A population-based study of 5.1 million Canadian adults living in Ontario. *Environ. Int.* **2019**, *132*, No. 105004.

(11) Pappin, A. J.; Christidis, T.; Pinault, L. L.; Crouse, D. L.; Brook, J. R.; Erickson, A.; Hystad, P.; Li, C.; Martin, R. V.; Meng, J.; Weichenthal, S.; van Donkelaar, A.; Tjepkema, M.; Brauer, M.; Burnett, R. T. Examining the Shape of the Association between Low Levels of Fine Particulate Matter and Mortality across Three Cycles of the Canadian Census Health and Environment Cohort. *Environ. Health Perspect.* **2019**, *127*, 107008.

(12) Burnett, R.; Chen, H.; Szyszkowicz, M.; Fann, N.; Hubbell, B.; Pope, C. A.; Apte, J. S.; Brauer, M.; Cohen, A.; Weichenthal, S.; Coggins, J.; di, Q.; Brunekreef, B.; Frostad, J.; Lim, S. S.; Kan, H.; Walker, K. D.; Thurston, G. D.; Hayes, R. B.; Lim, C. C.; Turner, M. C.; Jerrett, M.; Krewski, D.; Gapstur, S. M.; Diver, W. R.; Ostro, B.; Goldberg, D.; Crouse, D. L.; Martin, R. V.; Peters, P.; Pinault, L.; Tjepkema, M.; van Donkelaar, A.; Villeneuve, P. J.; Miller, A. B.; Yin, P.; Zhou, M.; Wang, L.; Janssen, N. A. H.; Marra, M.; Atkinson, R. W.; Tsang, H.; Quoc Thach, T.; Cannon, J. B.; Allen, R. T.; Hart, J. E.; Laden, F.; Cesaroni, G.; Forastiere, F.; Weinmayr, G.; Jaensch, A.; Nagel, G.; Concin, H.; Spadaro, J. V. Global estimates of mortality associated with long-term exposure to outdoor fine particulate matter. *Proc. Natl. Acad. Sci. U. S. A.* **2018**, *115*, 9592−9597.

(13) Anenberg, S. C.; Henze, D. K.; Tinney, V.; Kinney, P. L.; Raich, W.; Fann, N.; Malley, C. S.; Roman, H.; Lamsal, L.; Duncan, B.; Martin, R. V.; van Donkelaar, A.; Brauer, M.; Doherty, R.; Jonson, J. E.; Davila, Y.; Sudo, K.; Kuylenstierna, J. C. I. Estimates of the Global Burden jof Ambient PM2.5, Ozone, and NO2 on Asthma Incidence and Emergency Room Visits. *Environ. Health Perspect.* **2018**, *126*, 107004.

(14) Qiao, P.; Zhao, Y.; Cai, J.; van Donkelaar, A.; Martin, R.; Ying, H.; Kan, H. Twin growth discordance in association with maternal exposure to fine particulate matter and its chemical constituents during late pregnancy. *Environ. Int.* **2019**, *133*, No. 105148.

(15) Hazlehurst, M. F.; Carroll, K. N.; Loftus, C. T.; Szpiro, A. A.; Moore, P. E.; Kaufman, J. D.; Kirwa, K.; LeWinn, K. Z.; Bush, N. R.; Sathyanarayana, S.; Tylavsky, F. A.; Barrett, E. S.; Nguyen, R. H. N.; Karr, C. J. Maternal exposure to PM2.5 during pregnancy and asthma risk in early childhood: Consideration of phases of fetal lung development. *Environ. Epidemiol.* **2021**, *5*, No. e130.

(16) Di, Q.; Dai, L.; Wang, Y.; Zanobetti, A.; Choirat, C.; Schwartz, J. D.; Dominici, F. Association of Short-term Exposure to Air Pollution With Mortality in Older Adults. *JAMA* **2017**, *318*, 2446−2456.

(17) Pandey, P.; Khan, A. H.; Verma, A. K.; Singh, K. A.; Mathur, N.; Kisku, G. C.; Barman, S. C. Seasonal trends of PM2.5 and PM10 in ambient air and their correlation in ambient air of Lucknow city, India. *Bull. Environ. Contam. Toxicol.* **2012**, *88*, 265−270.

(18) Perrone, M. G.; Larsen, B. R.; Ferrero, L.; Sangiorgi, G.; De Gennaro, G.; Udisti, R.; Zangrando, R.; Gambaro, A.; Bolzacchini, E. Sources of high PM2.5 concentrations in Milan, Northern Italy: Molecular marker data and CMB modelling. *Sci. Total Environ.* **2012**, *414*, 343−355.

(19) Li, R.; Li, Z.; Gao, W.; Ding, W.; Xu, Q.; Song, X. Diurnal, seasonal, and spatial variation of PM2.5 in Beijing. *Sci. Bull.* **2015**, *60*, 387−395.

(20) Ford, B.; Heald, C. L. Exploring the uncertainty associated with satellite-based estimates of premature mortality due to exposure to fine particulate matter. *Atmos. Chem. Phys.* **2016**, *16*, 3499−3523.
(21) Jin, X.; Fiore, A. M.; Curci, G.; Lyapustin, A.; Civerolo, K.; Ku, M.; van Donkelaar, A.; Martin, R. V. Assessing uncertainties of a geophysical approach to estimate surface fine particulate matter distributions from satellite-observed aerosol optical depth. *Atmos. Chem. Phys.* **2019**, *19*, 295−313.
(22) van Donkelaar, A.; Martin, R. V.; Brauer, M.; Hsu, N. C.; Kahn, R. A.; Levy, R. C.; Lyapustin, A.; Sayer, A. M.; Winker, D. M. Global Estimates of Fine Particulate Matter using a Combined Geophysical-Statistical Method with Information from Satellites, Models, and Monitors. *Environ. Sci. Technol.* **2016**, *50*, 3762−3772.
(23) Bey, I.; Jacob, D. J.; Yantosca, R. M.; Logan, J. A.; Field, B. D.; Fiore, A. M.; Li, Q. B.; Liu, H. G. Y.; Mickley, L. J.; Schultz, M. G. Global modeling of tropospheric chemistry with assimilated meteorology: Model description and evaluation. *J. Geophys. Res.* **2001**, *106*, 23073−23095.
(24) Hand, J. L.; Prenni, A. J.; Schichtel, B. A.; Malm, W. C.; Chow, J. C. Trends in remote PM2.5 residual mass across the United States: Implications for aerosol mass reconstruction in the IMPROVE network. *Atmos. Environ.* **2019**, *203*, 141−152.
(25) World Health Organization Global Ambient Air Quality Database (Update 2018); https://www.who.int/airpollution/data/en/.
(26) Snider, G.; Weagle, C. L.; Murdymootoo, K. K.; Ring, A.; Ritchie, Y.; Stone, E.; Walsh, A.; Akoshile, C.; Anh, N. X.; Balasubramanian, R.; Brook, J.; Qonitan, F. D.; Dong, J.; Griffith, D.; He, K.; Holben, B. N.; Kahn, R.; Lagrosas, N.; Lestari, P.; Ma, Z.; Misra, A.; Norford, L. K.; Quel, E. J.; Salam, A.; Schichtel, B.; Segev, L.; Tripathi, S.; Wang, C.; Yu, C.; Zhang, Q.; Zhang, Y.; Brauer, M.; Cohen, A.; Gibson, M. D.; Liu, Y.; Martins, J. V.; Rudich, Y.; Martin, R. V. Variation in global chemical composition of PM2.5: emerging results from SPARTAN. *Atmos. Chem. Phys.* **2016**, *16*, 9629−9653.
(27) Snider, G. C.; Weagle, C. L.; Martin, R. V.; van Donkelaar, A.; Conrad, K.; Cunningham, D.; Gordon, C.; Zwicker, M.; Akoshile, C.; Artaxo, P.; Anh, N. X.; Brook, J.; Dong, J.; Garland, R. M.; Greenwald, R.; Griffith, D.; He, K.; Holben, B. N.; Kahn, R.; Koren, I.; Lagrosas, N.; Lestari, P.; Ma, Z.; Vanderlei Martins, J.; Quel, E. J.; Rudich, Y.; Salam, A.; Tripathi, S. N.; Yu, C.; Zhang, Y.; Zhang, Y.; Brauer, M.; Cohen, A.; Gibson, M. D.; Liu, Y. SPARTAN: A Global Network to Evaluate and Enhance Satellite-Based Estimates of Ground-Level Particulate Matter for Global Health Applications. *Atmos. Meas. Tech.* **2015**, *8*, 505−521.
(28) Brunsdon, C.; Fotheringham, A. S.; Charlton, M. E. Geographically Weighted Regression: A method for exploring spatial nonstationarity. *Geogr. Anal.* **1996**, *28*, 281−298.
(29) Giles, D. M.; Sinyuk, A.; Sorokin, M. G.; Schafer, J. S.; Smirnov, A.; Slutsker, I.; Eck, T. F.; Holben, B. N.; Lewis, J. R.; Campbell, J. R.; Welton, E. J.; Korkin, S. V.; Lyapustin, A. I. Advancements in the Aerosol Robotic Network (AERONET) Version 3 database − automated near-real-time quality control algorithm with improved cloud screening for Sun photometer aerosol optical depth (AOD) measurements. *Atmos. Meas. Tech.* **2019**, *12*, 169−209.
(30) Sayer, A. M.; Hsu, N. C.; Bettenhausen, C.; Jeong, M.-J. Validation and uncertainty estimates for MODIS Collection 6 "Deep Blue" aerosol data. *J. Geophys. Res. Atmos.* **2013**, *118*, 7864−7872.
(31) Sayer, A. M.; Hsu, N. C.; Bettenhausen, C.; Jeong, M.-J.; Holben, B. N.; Zhang, J. Global and regional evaluation of over-land spectral aerosol optical depth retrievals from SeaWiFS. *Atmos. Meas. Tech.* **2012**, *5*, 1761−1778.
(32) Levy, R. C.; Mattoo, S.; Munchak, L. A.; Remer, L. A.; Sayer, A. M.; Patadia, F.; Hsu, N. C. The Collection 6 MODIS aerosol products over land and ocean. *Atmos. Meas. Tech.* **2013**, *6*, 2989−3034.
(33) SEDAC http://sedac.ciesin.columbia.edu/data/collection/gpw-v4. (Jan 5, 2016),
(34) Zhang, F.; Wang, Z.-W.; Cheng, H.-R.; Lv, X.-P.; Gong, W.; Wang, X.-M.; Zhang, G. Seasonal variations and chemical characteristics of PM2.5 in Wuhan, central China. *Sci. Total Environ.* **2015**, *518-519*, 97−105.
(35) Liu, H.; Tian, H.; Zhang, K.; Liu, S.; Cheng, K.; Yin, S.; Liu, Y.; Liu, X.; Wu, Y.; Liu, W.; Bai, X.; Wang, Y.; Shao, P.; Luo, L.; Lin, S.; Chen, J.; Liu, X. Seasonal variation, formation mechanisms and potential sources of PM2.5 in two typical cities in the Central Plains Urban Agglomeration, China. *Sci. Total Environ.* **2019**, *657*, 657−670.
(36) Murari, V.; Kumar, M.; Mhawish, A.; Barman, S. C.; Banerjee, T. Airborne particulate in Varanasi over middle Indo-Gangetic Plain: variation in particulate types and meteorological influences. *Environ. Monit. Assess.* **2017**, *189*, 157.
(37) Rahman, M. H.; Sharma, V. P.; Kundu, S.; Datta, A. Seasonal Variation of Potential Source Locations of Atmospheric Particulates over the Indo-Gangetic Plain of India. *Open J. Air Pollut.* **2020**, *09*, 1−10.
(38) Jethva, H.; Torres, O.; Field, R. D.; Lyapustin, A.; Gautam, R.; Kayetha, V. Connecting Crop Productivity, Residue Fires, and Air Quality over Northern India. *Sci. Rep.* **2019**, *9*, 16594.
(39) Juda-Rezler, K.; Reizer, M.; Maciejewska, K.; Błaszczak, B.; Klejnowski, K. Characterization of atmospheric PM2.5 sources at a Central European urban background site. *Sci. Total Environ.* **2020**, *713*, No. 136729.
(40) Almeida, S. M.; Manousakas, M.; Diapouli, E.; Kertesz, Z.; Samek, L.; Hristova, E.; Šega, K.; Alvarez, R. P.; Belis, C. A.; Eleftheriadis, K. Ambient particulate matter source apportionment using receptor modelling in European and Central Asia urban areas. *Environ. Pollut.* **2020**, *266*, No. 115199.
(41) Miao, Y.; Li, J.; Miao, S.; Che, H.; Wang, Y.; Zhang, X.; Zhu, R.; Liu, S. Interaction Between Planetary Boundary Layer and $PM_{2.5}$ Pollution in Megacities in China: a Review. *Curr. Pollut. Rep.* **2019**, *5*, 261−271.
(42) Squizzato, S.; Masiol, M.; Brunelli, A.; Pistollato, S.; Tarabotti, E.; Rampazzo, G.; Pavoni, B. Factors determining the formation of secondary inorganic aerosol: a case study in the Po Valley (Italy). *Atmos. Chem. Phys.* **2013**, *13*, 1927−1939.
(43) Wang, C.; Yan, Y.; Niu, Y.; Li, R.; Xu, Y.; Hu, D.; Wu, J.; Peng, L. Formation and driving factors of sulfate in PM2.5 at a high-level atmospheric SO2 city of Yangquan in China. *Air Qual. Atmos. Health* **2021**, *14*, 491−501.
(44) Kiely, L.; Spracklen, D. V.; Wiedinmyer, C.; Conibear, L.; Reddington, C. L.; Archer-Nicholls, S.; Lowe, D.; Arnold, S. R.; Knote, C.; Khan, M. F.; Latif, M. T.; Kuwata, M.; Budisulistiorini, S. H.; Syaufina, L. New estimate of particulate emissions from Indonesian peat fires in 2015. *Atmos. Chem. Phys.* **2019**, *19*, 11105−11121.
(45) Verhegghen, A.; Eva, H.; Ceccherini, G.; Achard, F.; Gond, V.; Gourlet-Fleury, S.; Cerutti, P. O. The Potential of Sentinel Satellites for Burnt Area Mapping and Monitoring in the Congo Basin Forests. *Remote Sens.* **2016**, *8*, 986.
(46) Kambezidis, H. D.; Kaskaoutis, D. G. Aerosol climatology over four AERONET sites: An overview. *Atmos. Environ.* **2008**, *42*, 1892−1906.
(47) Artaxo, P.; Rizzo, L. V.; Brito, J. F.; Barbosa, H. M. J.; Arana, A.; Sena, E. T.; Cirino, G. G.; Bastos, W.; Martin, S. T.; Andreae, M. O. Atmospheric aerosols in Amazonia and land use change: from natural biogenic to biomass burning conditions. *Faraday Discuss.* **2013**, *165*, 203−235.
(48) Al-Taani, A. A.; Nazzal, Y.; Howari, F. M.; Yousef, A. Long-term trends in ambient fine particulate matter from 1980 to 2016 in United Arab Emirates. *Environ. Monit. Assess.* **2019**, *191*, 143.
(49) Laurent, B.; Marticorena, B.; Bergametti, G.; Léon, J. F.; Mahowald, N. M. Modeling mineral dust emissions from the Sahara desert using new surface properties and soil database. *J. Geophys. Res. Atmos.* **2008**, *113*, No. D14218.
(50) Sulaymon, I. D.; Mei, X.; Yang, S.; Chen, S.; Zhang, Y.; Hopke, P. K.; Schauer, J. J.; Zhang, Y. PM2.5 in Abuja, Nigeria: Chemical characterization, source apportionment, temporal variations, transport pathways and the health risks assessment. *Atmos. Res.* **2020**, *237*, No. 104833.

(51) Yang, X.; Zhao, C.; Yang, Y.; Fan, H. Long-term multi-source data analysis about the characteristics of aerosol optical properties and types over Australia. *Atmos. Chem. Phys.* **2021**, *21*, 3803−3825.
(52) Li, C.; McLinden, C.; Fioletov, V.; Krotkov, N.; Carn, S.; Joiner, J.; Streets, D.; He, H.; Ren, X.; Li, Z.; Dickerson, R. R. India Is Overtaking China as the World's Largest Emitter of Anthropogenic Sulfur Dioxide. *Sci. Rep.* **2017**, *7*, 14304.
(53) Wang, N.; Lyu, X.; Deng, X.; Huang, X.; Jiang, F.; Ding, A. Aggravating O3 pollution due to NOx emission control in eastern China. *Sci. Total Environ.* **2019**, *677*, 732−744.
(54) Chan, E. A. W.; Gantt, B.; McDow, S. The reduction of summer sulfate and switch from summertime to wintertime PM(2.5) concentration maxima in the United States. *Atmos. Environ.* **2018**, *175*, 25−32.
(55) Ridley, D. A.; Heald, C. L.; Ridley, K. J.; Kroll, J. H. Causes and consequences of decreasing atmospheric organic aerosol in the United States. *Proc. Natl. Acad. Sci. U. S. A.* **2018**, *115*, 290−295.
(56) Dionisio, K. L.; Arku, R. E.; Hughes, A. F.; Vallarino, J.; Carmichael, H.; Spengler, J. D.; Agyei-Mensah, S.; Ezzati, M. Air Pollution in Accra Neighborhoods: Spatial, Socioeconomic, and Temporal Patterns. *Environ. Sci. Technol.* **2010**, *44*, 2270−2276.
(57) Bauer, S. E.; Im, U.; Mezuman, K.; Gao, C. Y. Desert Dust, Industrialization, and Agricultural Fires: Health Impacts of Outdoor Air Pollution in Africa. *J. Geophys. Res.: Atmos.* **2019**, *124*, 4104−4120.
(58) Apte, J. S.; Marshall, J. D.; Cohen, A. J.; Brauer, M. Addressing Global Mortality from Ambient PM2.5. *Environ. Sci. Technol.* **2015**, *49*, 8057−8066.

https://doi.org/10.1021/acs.est.1c05309
Environ. Sci. Technol. 2021, 55, 15287−15300